Modeling of thermodynamic fluctuations in canonical shock-turbulence interaction

Yogesh Prasaad M. S.* and Krishnendu Sinha†
Department of Aerospace Engineering, Indian Institute of Technology Bombay, Mumbai 400 076, India

Interaction of a shock wave with turbulence can generate large thermodynamic fluctuations in a flow. This can lead to enhanced mixing, peak heat transfer and high sound level. The canonical interaction of homogeneous isotropic turbulence with a nominally normal shock wave acts as a model problem to investigate physics and develop predictive models. The case of purely vortical turbulence upstream of the shock is arguably the most fundamental case and it is the focus of the current work. We use direct numerical simulation (DNS) data and linear interaction analysis (LIA) to develop a predictive model for the thermodynamic field. Specifically, transport equation-based models are proposed for the variances in temperature, pressure, density and entropy. The jump in the thermodynamic variances are modeled in terms of the mean compression at the shock, and the closure coefficients are obtained via Kovásznay mode decomposition. By comparison, the downstream decay is modeled in a phenomenological way in terms of acoustic transient near the shock and a far-field decay due to viscous dissipation. The model predictions are found to match well with available DNS data for a range of shock strengths. In addition, the closed-form solution of the model equations give the scaling of the thermodynamic fluctuations with mean flow Mach number.

Nomenclature

a	=	sound speed, m/s
c_p & c_v	=	gas specific heat at constant pressure and constant volume, respectively, J/(kg.K)
k	=	turbulent kinetic energy, $k \equiv \overline{u_i' u_i'}/2$, m^2/s^2
L_ϵ	=	dissipation lengthscale, $L_\epsilon \equiv k^{3/2} \,/\, \epsilon$, m
M	=	Mach number, $M \equiv \bar{u} \,/\, \bar{a}$
M_t	=	turbulent Mach number, $M_t \equiv \sqrt{\overline{u_i' u_i'}} \,/\, \bar{a}$
p	=	pressure, Pa
r	=	mean compression by the shock, $r \equiv \bar{u}_1 \,/\, \bar{u}_2 \equiv \bar{\rho}_2 \,/\, \bar{\rho}_1$

*Graduate student, Department of Aerospace Engineering, Indian Institute of Technology Bombay.
†Professor, Department of Aerospace Engineering, Indian Institute of Technology Bombay, and AIAA Senior Member.

R = specific gas constant, J/(kg.K)

Re_λ = Reynolds number based on Taylor lengthscale, $Re_\lambda \equiv \rho\, u'\, \lambda \,/\, \mu$

s = entropy, J/(kg.K)

T = temperature, K

u = streamwise velocity, m/s

x = coordinate for the streamwise direction, m

ϵ = dissipation rate of turbulent kinetic energy, m^2/s^3

γ = ratio of gas specific heats, $\gamma \equiv c_p \,/\, c_v$

κ_0 = inflow turbulence peak energy wavenumber, $1/m$

λ = Taylor lengthscale, m

μ = dynamic viscosity, kg/(m.s)

ρ = density, kg/m^3

ξ_t = shock-unsteadiness velocity, m/s

Subscripts

$(.)_0$ = inlet value

$(.)_1$ = shock-upstream value

$(.)_2$ = shock-downstream value

Superscripts

$(.)^*$ = dimensional variable

$\overline{(.)}$ = Reynolds-averaged variable

$(.)'$ = fluctuations around the Reynolds-averaged variable

I. Introduction

Interaction of shock waves with flow turbulence is a common feature in the supersonic and hypersonic regime. Shock turbulence interaction is important in a variety of applications, viz. high-speed propulsion systems [1], inertial confinement fusion [2, 3], shock wave lithotripsy, and astrophysical shock waves [4, 5]. Shock waves can significantly enhance turbulent mixing [6], Reynolds stresses [7], vorticity fluctuations or enstrophy [8] and turbulent transfer of heat [9]. The canonical interaction of a normal shock with homogeneous isotropic turbulence serves as a model problem to gain physical insight into the phenomena. It has been the subject of a large number of numerical [6, 10–12], theoretical [5, 13–16] and experimental works [17–19].

The primary effect of a shock wave is to amplify the turbulent velocity and vorticity fluctuations in the flow [20]. The rapid one-dimensional compression can impart significant anisotropy to the Reynolds stress tensor [12, 21]. This is

associated with a reduction in the Kolmogorov length scale and the transfer of energy to higher wavenumbers. A shock wave can also lead to large fluctuations in pressure, density and temperature of the gas. Thermodynamic fluctuations play a vital role in turbulent mass flux, turbulent heat transfer, and in the transport of energy between internal and kinetic energy components [22]. Shock-induced thermodynamic fluctuations are therefore being studied in relation to Richtmyer-Meshkov instability [2, 3], jet noise [23, 24] and surface heat flux [9, 25]. In scramjet combustion, shock waves are essential for rapid mixing of the fuel by turbulence generation [26, 27]. Additionally, the temperature rise induced due to the shock wave(s) results in spontaneous ignition of the fuel-air mixture [1, 28].

In a recent work [29], we used direct numerical simulation to study the thermodynamic field in canonical shock-turbulence interaction. Homogeneous isotropic turbulence, with negligible pressure, temperature and density fluctuations, is fed into a one-dimensional mean flow through a shock wave. The shock is nominally normal and steady in a time-averaged sense, but deforms and oscillates in response to the unsteady turbulent fluctuations going through it. Statistics computed behind the shock wave are used to study the effect of mean compression as well the evolution of the thermodynamic field with downstream distance. It is found that the temperature and pressure variances can take very large values, followed by a rapid exponential decay behind the shock. By comparison, the density variance can have a non-monotonic behaviour at high Mach numbers, followed by a gradual decay far away from the shock.

Sethuraman et al. [29] also use a theoretical tool called the linear interaction analysis (LIA) to investigate the post-shock thermodynamic field. The procedure uses a linear and inviscid framework, valid for small turbulent fluctuations and high Reynolds number. The analysis is based on Kovásznay decomposition [30] of the disturbance field into vortical, acoustic and entropy components. Interaction of an elementary vorticity wave generates all three modes downstream, and the post-shock solution is a function of shock strength and the incident wave properties. Homogeneous isotropic turbulence upstream of the shock is simulated by integrating over a range of wavenumbers and incidence angles, for a prescribed energy spectrum, say the von Kármán spectrum,

$$E(k) \sim \frac{1}{k_0} \frac{(k/k_0)^4}{\left[(k/k_0)^2 + 5/6\right]^{11/6}}. \tag{1}$$

Downstream statistics are compared with DNS data, and it is found that LIA can capture the main effects of the shock interaction. These include the effects of bulk compression, generation of acoustic energy at the shock and its rapid decay immediately behind the shock.

In this paper, we use the physical understanding gained via DNS and LIA to propose models to predict the level of post-shock thermodynamic fluctuations. We consider four fundamental quantities, namely, the variances in temperature, pressure, density and entropy ($s/c_v = \ln(p/\rho^\gamma)$), to capture the essence of the entire thermodynamic field. The objective is to predict the jump in the four variances across the shock, as well as their downstream evolution. We develop transport equation based models for the thermodynamic variances and use Kovásznay mode decomposition to find

closure coefficients. The model predictions are compared with available DNS data with a focus on the effect of shock strength. The procedure followed is similar to the $k - \epsilon$ model developed by Sinha et al. [8, 31], which has found application in a variety of shock-dominated flows [32–38].

We note that the majority of existing turbulence models are for the turbulent kinetic energy and its dissipation rate, and the Reynolds stress tensor. Limited attempts have been made to develop transport equation models for temperature and pressure fluctuations and related quantities [3, 39–41]. There are virtually no turbulence models to capture the effect of shock waves on thermodynamic fluctuations – an important phenomenon in high-speed flows, and the current work is an attempt to fill this void. The only exception is the model by Quadros & Sinha [42] to predict the turbulent heat flux in canonical shock-turbulence interaction. A variable turbulent Prandtl number form of the same [43] has been successful in predicting the peak surface heat transfer rates in shock-boundary layer interactions [37].

II. Thermodynamic variances behind the shock

Figure 1, adapted from Ref. [29], shows the variation of pressure, temperature, density and entropy variance in a canonical shock-turbulence interaction. The normal shock is located at $x = 0$ and the grey region corresponds to the unsteady oscillations of the shock wave. The thermodynamic variances have negligible value upstream of the shock wave ($x < 0$), owing to the vortical nature of the incoming turbulence field. We non-dimensionalize the thermodynamic variances by their respective local mean values, and the upstream turbulence kinetic energy by the square of the upstream mean flow velocity. The entropy variance is non-dimensionalized by the square of the specific heat of the gas at constant pressure (with $\gamma = 1.4$). The data presented in the figure are further normalized by the upstream turbulent kinetic energy, so as to assess the effect of the shock compression relative to the incoming turbulence intensity. The streamwise coordinate is non-dimensionalized by the upstream peak energy wavenumber, κ_0.

The post-shock variances in the thermodynamic quantities, as obtained from DNS, show interesting trends. The pressure and temperature variances attain high values at the shock wave, followed by a rapid drop immediately behind the shock. The pressure fluctuations reach a non-zero asymptotic value far downstream, whereas the temperature variance continues to decay in the far-field. The LIA results mimic the trend in the pressure well, and match the far-field value closely. For the temperature variance, LIA is able to capture the rapid drop behind the shock. This corresponds to the near-field acoustic decay [29] that is a characteristic feature of canonical shock-turbulence interaction. The acoustic decay is an inviscid mechanism and is reproduced well by LIA. In the absence of viscous effects, LIA predicts a finite far-field value for $\overline{T'^2}$. The DNS data, on the other hand, shows a systematic deviation from the LIA predictions. In fact, the data shows a clear transition between the rapid acoustic decay and the slow viscous dissipation of $\overline{T'^2}$ at $\kappa_0 x \simeq 1$.

The DNS density variance plotted in Fig. 1(c) has a non-monotonic variation with a local peak behind the shock (at $\kappa_0 x \simeq 1$). As per LIA, $\overline{\rho'^2}$ starts at a low value, increases behind the shock and then attains an asymptotic level farther away. Once again, there is a good match between DNS and LIA in the near-field ($\kappa_0 x < 1$), and it is attributed to the

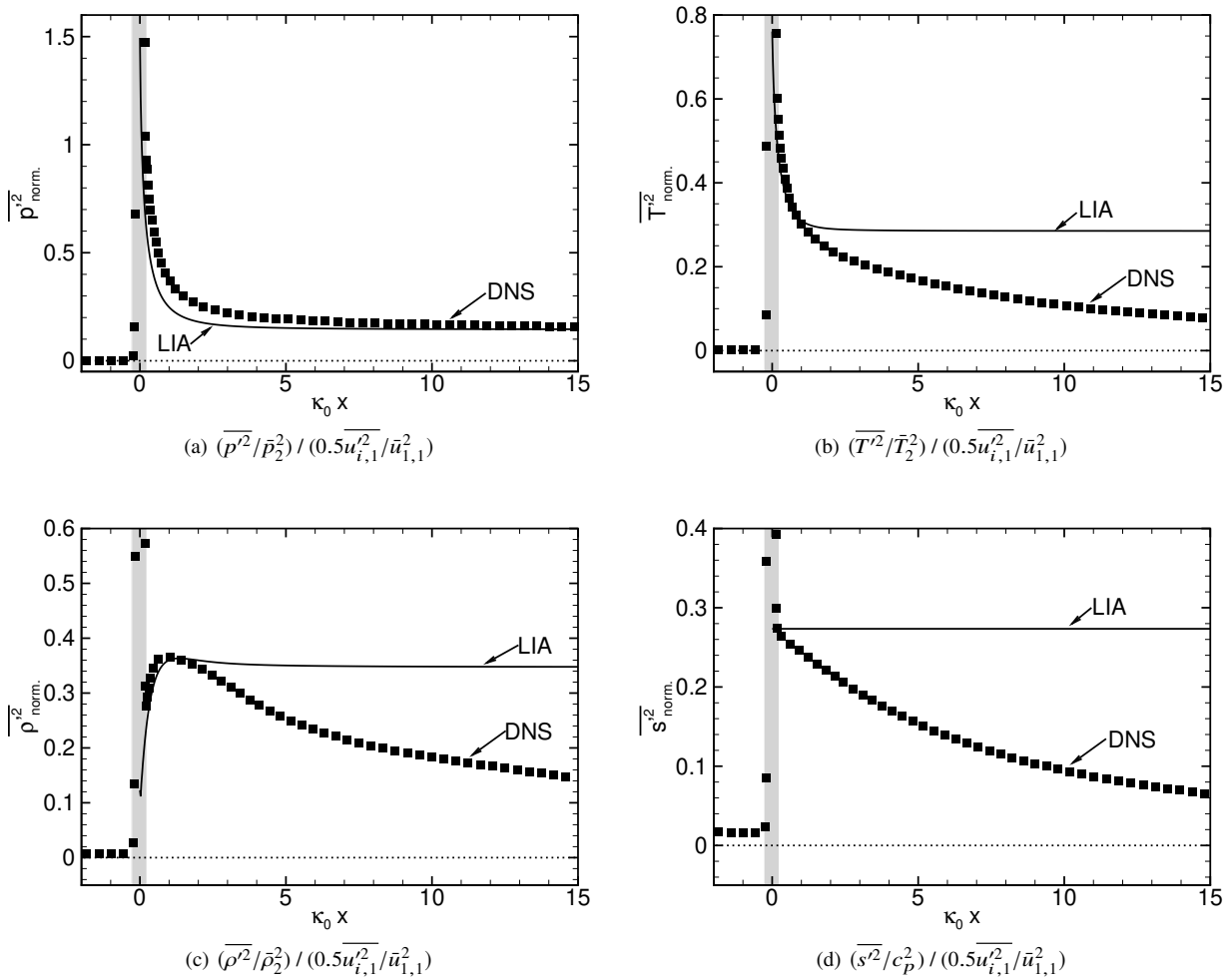

(a) $(\overline{p'^2}/\bar{p}_2^2) / (0.5\overline{u_{i,1}'^2}/\bar{u}_{1,1}^2)$

(b) $(\overline{T'^2}/\bar{T}_2^2) / (0.5\overline{u_{i,1}'^2}/\bar{u}_{1,1}^2)$

(c) $(\overline{\rho'^2}/\bar{\rho}_2^2) / (0.5\overline{u_{i,1}'^2}/\bar{u}_{1,1}^2)$

(d) $(\overline{s'^2}/c_p^2) / (0.5\overline{u_{i,1}'^2}/\bar{u}_{1,1}^2)$

Fig. 1 Spatial variation of normalized thermodynamic variances for $M = 3.50$, $M_t = 0.15$ and $Re_\lambda = 33$ shock-turbulence interaction.

inviscid acoustic adjustment behind the shock. The non-monotonic behaviour is due to a negative correlation between the acoustic and entropy modes that contributes to the density fluctuations. In fact, the density plot bears resemblance to the turbulent kinetic energy variation behind a shock wave (see Fig. 9 in Ref. [12]). A similar interaction between the acoustic and vortical modes is used to explain the trend in TKE [11, 20]. Farther downstream, the DNS data shows a gradual decrease in $\overline{\rho'^2}$, which is similar to the viscous decay of the temperature variance.

The entropy variance computed from the DNS solution (Fig. 1(d)) attains very high values in the region of shock oscillations. This is an artefact of the unsteady shock motion, and not turbulent fluctuations in a conventional way. The same is true for the other thermodynamic variances presented in Fig. 1. At the edge of the mean shock, the DNS $\overline{s'^2}$ matches the LIA result. Behind the shock, LIA predicts a constant $\overline{s'^2}$, because entropy fluctuations are not affected by the rapid acoustic adjustment in the near-field. Entropy is a pure mode as per Kovásznay's analysis for small perturbations in an uniform inviscid flow and evolves independent of the acoustic phenomena in the flow. The entropy

variance exhibits a slow viscous decay with distance from the shock wave. This is corroborated by the budget of the transport equation for $\overline{s'^2}$ in Ref. [29], where the viscous dissipation is the dominant term behind the shock. This is not true for the other thermodynamic variances presented in Fig. 1, as explained below.

As per LIA, pressure fluctuations are due to the acoustic mode and do not display the slower decay found in the entropy variance. On the other hand, temperature and density fluctuations have contribution from both the acoustic and entropy modes. The acoustic mode is found to be dominant in the near-field, and it decays rapidly to low level at the end of the acoustic adjustment region ($\kappa_0 x \lesssim 2$). LIA predicts a finite and constant amplitude of the entropy mode with streamwise distance, and is therefore the main contributor to the thermodynamic field away from the shock. The far-field value of $\overline{T'^2}$ and $\overline{\rho'^2}$ are thus governed by the entropy component, and they exhibit a slow viscous decay similar to the entropy variance. The DNS budget of the temperature variance transport equation (Fig. 20 in Ref. [29]) clearly shows this effect. Inviscid dilatational source terms are dominant near the shock, while the viscous dissipation is important far away.

The data presented in Fig. 1 clearly shows that LIA and DNS can be together used to develop predictive models for computational fluid dynamic simulation. As seen in the figure, the near-field values of the density, pressure, and temperature variances are effectively captured by LIA, and the theoretical framework can be reliably used in this region. The linear and inviscid approximations inherent in LIA often lead to substantial simplification in the equations governing the thermodynamic fluctuations. The dominant physical mechanisms can thus be easily identified, and used for model development. The downstream decay, on the other hand, can be modeled in terms of the post-shock turbulent dissipation rate [8] and calibrated to the DNS data. A similar procedure applied to turbulence kinetic energy [31] led to the modeling of unsteady shock oscillations based on LIA theory. The resulting shock-unsteadiness $k - \epsilon$ model could match the post-shock TKE in the DNS of canonical shock-turbulence interaction.

III. Model development

In this section, we develop transport-equation based models for the thermodynamic variances. The approach consists of two parts, as delineated above. First, we model the jump in the thermodynamic variances across the shock wave and compare the model predictions with DNS data as a function of Mach number. We focus on Mach numbers higher than two, as the post-shock thermodynamic variances are too small in magnitude for weaker shocks. Of particular interest is the high Mach number scaling of the thermodynamic field, which is derived as the solution of the model equations in the limit $M \to \infty$. As a second step, we model the evolution of the thermodynamic variances downstream of the shock. Both the acoustic transient, as well as the viscous decay are modeled in a phenomenological way. The model predictions are finally compared with DNS data in the entire domain, namely, upstream and downstream of the shock and in the vicinity of the shock wave.

A. Temperature variance

We start with a transport equation for the temperature variance derived using the conservation of total enthalpy across a shock wave. It is written in terms of the fluctuations in temperature T' and shock-normal velocity u'

$$c_p \frac{\partial T'}{\partial x} = -(u' - \xi_t) \frac{\partial \bar{u}}{\partial x} - \bar{u} \frac{\partial u'}{\partial x}. \tag{2}$$

Here $x = \xi(y, z, t)$ is the instantaneous position of the locally unsteady shock wave, such that $\xi_t = \partial \xi / \partial t$ is the instantaneous shock velocity in the stream wise direction. The equation is written in the shock frame of reference, such that $(u' - \xi_t)$ is the turbulent fluctuation relative to the unsteady shock wave. Note that the terms that are linear in the turbulent fluctuations are retained, while the higher-order terms are neglected, under the assumption of small fluctuation magnitude relative to the corresponding mean flow quantities.

Taking a moment of the above equation with T' and Reynolds averaging, we get

$$c_p \frac{\partial}{\partial x} \left(\frac{\overline{T'^2}}{2} \right) = -\overline{u'T'} \frac{\partial \bar{u}}{\partial x} + \overline{T'\xi_t} \frac{\partial \bar{u}}{\partial x} - \bar{u} \overline{T' \frac{\partial u'}{\partial x}}. \tag{3}$$

The first term on the right hand side is the production of temperature fluctuations due to mean compression. It represents the transfer of energy from the mean kinetic energy to fluctuating internal energy. Physical insight can be derived from Eq. (2), where a positive velocity fluctuation (with a negative $\partial \bar{u} / \partial x$) leads to an increase in T', i.e., $\partial T' / \partial x > 0$. Starting with an upstream $T' = 0$ would thus give a positive T' for $u' > 0$ and a negative T' for $u' < 0$. Thus, the correlation between the velocity and temperature fluctuations is expected to be positive, and it leads to a positive production effect in the $\overline{T'^2}$ equation (3).

The second term represents the shock-unsteadiness mechanism, and brings in the net effect of an oscillating shock wave on the temperature field. It is similar in form, but opposite in sign to the production term in Eq. (3), with $\overline{T'\xi_t}$ replacing the velocity-temperature correlation. In this respect, it appears analogous to the shock-unsteadiness effect in the TKE equation [31], which leads to a damping of the turbulent amplification by the shock. The last source term brings in the effect of the dilatational fluctuations generated by the shock; note that the upstream velocity field is purely rotational, as per the incompressible vorticity mode. Across the shock, a positive $\partial u' / \partial x$ in Eq. (2), with a positive mean velocity, gives a negative temperature fluctuation, and vice versa. The correlation $\overline{T' (\partial u' / \partial x)}$ in Eq. (3) is thus negative, and it is expected to have a positive contribution to the temperature variance.

The Rankine-Hugoniot jump conditions across an unsteady shock wave can be linearized to get the following relation for the temperature fluctuation.

$$c_p \left(T_2' - T_1' \right) = -\left(u_2' - \xi_t \right) \left(\bar{u}_2 - \bar{u}_1 \right) - \bar{u}_1 \left(u_2' - u_1' \right) \tag{4}$$

Here, subscript 1 and 2 correspond to the shock upstream and downstream locations. This can be interpreted as an integrated form of Eq. (2) across the shock wave. On multiplying each term by $T'_m = (T'_1 + T'_2)/2$, we get an equation that is analogous to the transport equation of the temperature variance at the shock wave.

$$c_p \frac{\left(\overline{T'^2_2} - \overline{T'^2_1}\right)}{2} = \underbrace{-\overline{u'_1 T'_m}\,(\bar{u}_2 - \bar{u}_1)}_{\text{Production}} + \underbrace{\overline{T'_m \xi_t}\,(\bar{u}_2 - \bar{u}_1)}_{\text{Shock-unsteadiness}} \underbrace{- \bar{u}_2\,\overline{T'_m\left(u'_2 - u'_1\right)}}_{\text{Dilatation}}, \tag{5}$$

The left-hand side represents the change in $\overline{T'^2}$ across the shock, and the terms on the right-hand side match up, one to one, with the source terms in Eq. (3). They consist of the upstream and downstream mean flow quantities, which are a function of the mean flow Mach number. The turbulence correlations can be computed from the LIA solution for the three-dimensional disturbance field obtained for each Mach number. The different terms in Eq. (5) can thus be computed and interpreted as an integrated budget of the differential transport equation (3) across a shock wave.

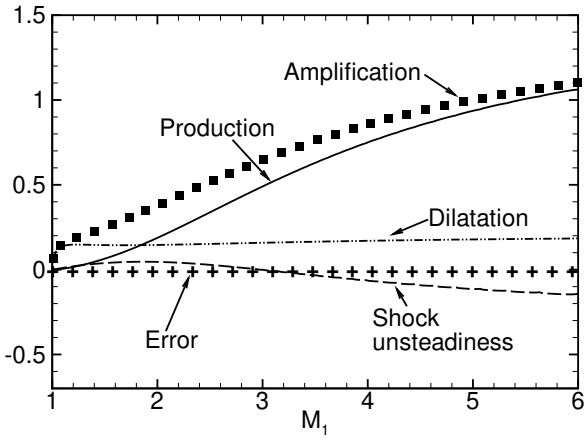

Fig. 2 Budget of temperature variance equation (5) **across a normal shock for varying Mach numbers.**

Figure 2 shows the LIA budget of Eq. (5) plotted as a function of shock strength, where the error denotes the difference between the LHS and RHS. All the terms are normalized by $c_p\,\overline{T}_2^2\,(k_1/\bar{u}_1^2)$ in line with the normalization described in Sec. II. The production due to mean compression is found to be the dominant mechanism for the generation of temperature fluctuations at the shock. The dilatation term albeit small, is finite and is responsible for the amplification of temperature variance at low Mach numbers. The shock-unsteadiness term is found to be relatively small, except for the high Mach number cases, where it balances the contribution from the dilatation term. The production mechanism contributes entirely to the temperature variance behind the shock in the hypersonic limit.

Retaining only the production term in the $\overline{T'^2}$ equation (3), and modeling the temperature flux $\overline{u'T'}$ as per [42] (details in Appendix B), we get

$$\frac{\partial \overline{T'^2}}{\partial x} = -2\,\frac{\overline{u'T'}}{c_p}\,\frac{\partial \bar{u}}{\partial x} = -2\,C_{uT}\,\frac{k\,\bar{u}}{c_p^2}\,\frac{\partial \bar{u}}{\partial x}, \tag{6}$$

which can be integrated along with the k equation (without ϵ term) given in Appendix A, to obtain the following closed-form solution for the temperature variance downstream of the shock wave.

$$\overline{T_2'^2}_{norm.} = \frac{\overline{T'^2}}{\bar{T}_2^2\,(k_1/\bar{u}_1^2)} \simeq \frac{3\,C_{uT}}{(b_1'+2)}\left[1 - r^{-\frac{2}{3}(2+b_1')}\right](\gamma-1)^2\,\frac{M_1^4}{T_r^2}, \tag{7}$$

Here, C_{uT} and b_1' are the model coefficients defined in Appendix B, $r = \bar{u}_1/\bar{u}_2 = \bar{\rho}_2/\bar{\rho}_1$ is the mean compression by the shock and $T_r = \bar{T}_2/\bar{T}_1$ is the mean temperature ratio across the shock wave. A purely vortical upstream turbulence has $T_1' \simeq 0$ and in the limit $M_1 \to 1$, the density ratio r approaches 1, which results in $T_2' \to 0$. There is negligible temperature fluctuations generated by very weak shocks. In the high Mach number range, $r \to (\gamma+2)/(\gamma-1)$ and we get $\overline{T_2'^2} \propto M_1^4/T_r^2$. Noting that $T_r \propto M_1^2$, the normalized temperature variance approaches a finite asymptotic value. This is consistent with LIA predictions presented in Ref. [29]. The magnitude of the post-shock temperature fluctuations thus scales with the downstream mean temperature for a fixed turbulence intensity $(k_1/\bar{u}_1^2)$ upstream of the shock. For a given freestream temperature $\bar{T}_1$, strong shocks at hypersonic Mach numbers can generate large magnitude of temperature fluctuations ($T_2'^2 \propto \bar{T}_2 \propto M_1^2\,\bar{T}_1$), proportional to the square of the shock Mach number.

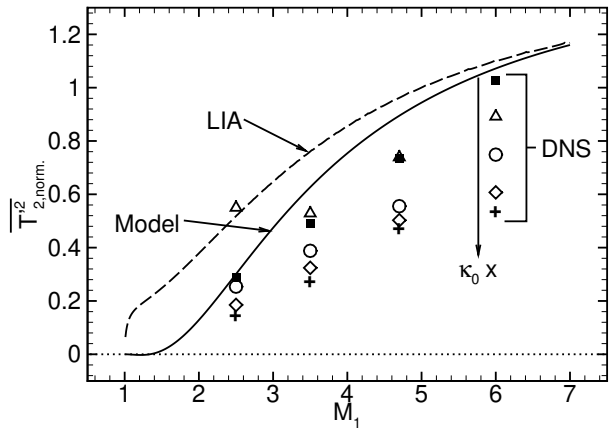

Fig. 3 Variation of normalized temperature variance against Mach number as obtained from DNS, LIA and model equation (7)**. Normalization is by the factor,** $\bar{T}_2^2\,(k_1/\bar{u}_1^2)$**.**

Figure 3 compares the model predictions along with LIA and DNS results. Ideally, we would like to assess the model against the peak value in DNS, but the rapid variation of $\overline{T'^2}$ behind the shock makes is difficult (see Fig. 1). Instead, we present DNS data at different x locations: at the shock edge identified from mean dilatation profile (filled squares), $\kappa_0 x = 0.25$ (triangles), $\kappa_0 x = 0.5$ (circles), $\kappa_0 x = 0.75$ (diamonds), and $\kappa_0 x = 1$ (plusses). All the data show the same monotonic trend with Mach number, as the model prediction. The only exception is the $\kappa_0 x = 0.25$ value for $M_1 = 2.5$ case, which may be due to high unsteady shock oscillations at low Mach number. The model predictions are in general higher than the DNS data; the closest match is obtained with the mean shock edge values at the lowest and

highest Mach numbers. The LIA near-field value (at $\kappa_0 x = 0^+$) is comparable to the model predictions in the hypersonic range ($M_1 > 5$). At low Mach numbers, the LIA solution is qualitatively different from the model results. This is because of the dilatation term in Eq. (3), which is not included in the simplified model equation. The magnitude of post-shock $\overline{T'^2}$ is relatively small for such weak interactions.

B. Pressure variance

A transport equation for $\overline{p'^2}$ is derived by taking a moment of the shock-normal momentum equation with p' and Reynolds averaging.

$$\frac{\partial}{\partial x}\left(\frac{\overline{p'^2}}{2}\right) = -\bar{\rho}\,\overline{p'u'}\,\frac{\partial \bar{u}}{\partial x} - \bar{u}\,\overline{p'\rho'}\,\frac{\partial \bar{u}}{\partial x} + \bar{\rho}\,\overline{p'\xi_t}\,\frac{\partial \bar{u}}{\partial x} - \bar{\rho}\,\bar{u}\,\overline{p'\frac{\partial u'}{\partial x}}, \tag{8}$$

Once again, viscous and higher order terms are neglected in line with the linear inviscid approximation in the vicinity of the shock wave. Also, note that the shock-parallel derivatives are assumed to be small compared to those in the shock-normal direction. An integrated form can be derived in a similar way by starting with the linearized Rankine-Hugoniot jump condition for pressure fluctuations at the shock. Taking a moment with $p'_m = \left(p'_1 + p'_2\right)/2$ and Reynolds averaging gives us

$$\frac{\overline{p_2'^2} - \overline{p_1'^2}}{2} = -\underbrace{\bar{\rho}_1\,\overline{p'_m u'_1}\,(\bar{u}_2 - \bar{u}_1)}_{\text{Production-1}} - \underbrace{\bar{u}_1\,\overline{p'_m \rho'_1}\,(\bar{u}_2 - \bar{u}_1)}_{\text{Production-2}} + \underbrace{\bar{\rho}_1\,\overline{p'_m \xi'_t}\,(\bar{u}_2 - \bar{u}_1)}_{\text{Shock-unsteadiness}} - \underbrace{\bar{\rho}_1\,\bar{u}_1\,\overline{p'_m\left(u'_2 - u'_1\right)}}_{\text{Dilatation}}, \tag{9}$$

where the different terms are identified as per the physical mechanisms they represent.

The terms on the right-hand side of Eq. (8) and (9) are analogous to the corresponding terms in the temperature variance equations (3) and (4), respectively. There is an extra $\bar{\rho}_1$ in the $\overline{p'^2}$ source terms to match the dimensions of the pressure equation. The only addition is the second production term, but it is identically zero for purely vortical turbulence ($\rho'_1 = 0$) upstream of the shock wave. The budget of Eq. (9) computed using LIA data exhibits several similarities with the $\overline{T'^2}$ budget in Fig. 1. See Fig. 3 in Ref. [44]; it is not included here. Specifically, the production term increases with Mach number to become the largest term for strong interactions, while the shock-unsteadiness term is comparatively small. The dilatation term is large at low Mach numbers and its magnitude exceeds the corresponding term for the temperature variance.

A modeled transport equation for the pressure variance is proposed by including the effect of the production term

$$\frac{\partial \overline{p'^2}}{\partial x} \approx -2\,\bar{\rho}\,\overline{p'u'}\,\frac{\partial \bar{u}}{\partial x}, \tag{10}$$

and neglecting the dilatation effect, as in the $\overline{T'^2}$ case. The objective to arrive at the simplest possible model equation to predict the post-shock $\overline{p'^2}$ at high Mach numbers. A closure model for $\overline{p'u'}$ is obtained by using the isentropic relation

between pressure and temperature fluctuations

$$\frac{p'}{\bar{p}} = \left(\frac{\gamma}{\gamma-1}\right)\frac{T'}{\bar{T}},$$

such that

$$\overline{p'u'} = \left(\frac{\gamma}{\gamma-1}\right)\frac{\bar{p}}{\bar{T}}\,\overline{u'T'} = \left(\frac{\gamma}{\gamma-1}\right)\frac{\bar{p}}{\bar{T}}\,C_{uT}\,\frac{k\,\bar{u}}{c_p}, \tag{11}$$

where the model for $\overline{u'T'}$ is inserted as per Eq. (43). This is justified by the Kovásznay mode decomposition of the downstream thermodynamic field. The pressure field is assumed to be purely acoustic. The near-field temperature fluctuations are also dominated by the acoustic mode, even for strong shocks. This is corroborated by the fact that both $\overline{p'^2}$ and $\overline{T'^2}$ have a rapid monotonic drop (see Fig. 1) behind the shock wave, for all Mach numbers.

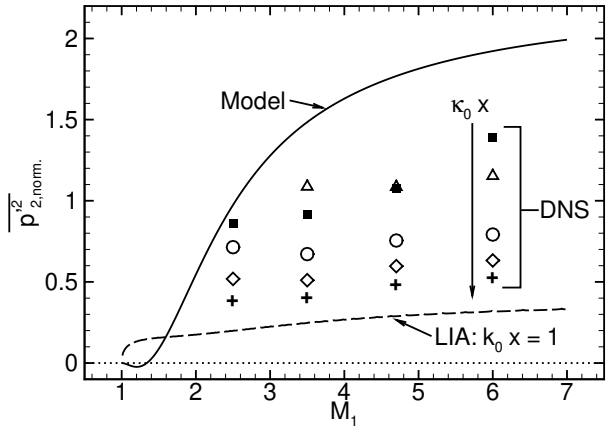

Fig. 4 Variation of normalized pressure variance against Mach number from DNS, model equation (12) **and LIA at** $\kappa_0 x = 1$ **location. Normalization is by the factor,** $\bar{p}_2^2\,(k_1/\bar{u}_1^2)$**.**

Substituting Eq. (11) in the model Eq. (10) and integrating across the shock gives us

$$\overline{p_2'^2}_{norm.} = \frac{\overline{p'^2}}{\bar{p}_2^2\,(k_1/\bar{u}_1^2)} \simeq \frac{3\,C_{uT}}{(b_1'-1)}\left[1 - r^{-\frac{2}{3}(b_1'-1)}\right]\gamma^2\,\frac{M_1^4}{p_r^2}, \tag{12}$$

which has a functional form similar to the normalized temperature variance in Eq. (7). Here, $p_r = \bar{p}_2/\bar{p}_1$ is the pressure ratio across the shock and $p_r \propto M_1^2$ in the high Mach number limit. The pressure fluctuations thus scale with the mean post-shock pressure for fixed upstream values of $\bar{p}_1$, $\bar{u}_1$ and k_1. The model predicts $p'_{2,rms} \simeq \sqrt{2\,k_1}\,\bar{p}_2/\bar{u}_1$ for $M_1 \to \infty$, and it is substantially higher than the DNS data (see Fig. 4). The DNS values are taken at different $\kappa_0 x$ locations, similar to Fig. 3 (same legend), owing to the rapid monotonic variation of $\overline{p'^2}$ behind the shock. LIA results are plotted at $\kappa_0 x = 1$. The DNS data, as expected, shows a steady decrease between $\kappa_0 x = 0.25$ and 1. The model prediction at $x = 0^+$ and the LIA results at $\kappa_0 x = 1$ seem to bracket the DNS data. For low Mach numbers ($M < 1.3$),

the model equation predicts $\overline{p_2'^2} < 0$ and is therefore unphysical. The limitation of the model can possibly be attributed to neglecting the pressure-dilatation effect in Eq. (8).

C. Density variance

A transport equation for the density variance can be obtained by taking a moment of the linearized mass conservation equation across a shock wave.

$$\overline{u}\,\frac{\partial}{\partial x}\left(\frac{\overline{\rho'^2}}{2}\right) = -\overline{u'\rho'}\,\frac{\partial\overline{\rho}}{\partial x} - \overline{\rho'^2}\,\frac{\partial\overline{u}}{\partial x} + \overline{\rho'\xi_t}\,\frac{\partial\overline{\rho}}{\partial x} - \overline{\rho}\,\overline{\left(\rho'\frac{\partial u'}{\partial x}\right)}, \tag{13}$$

The source terms on the right-hand side bear strong resemblance to those in the $\overline{T'^2}$ equation (3). The analogous terms are production due to mean compression (first term), shock-unsteadiness term (third term) and dilatation effect (last term). The additional production due to $\overline{\rho'^2}$ (second term) is expected to be small in the absence of upstream density fluctuations.

Following an approach similar to the temperature variance, we propose a simple modeled form of the transport equation

$$\frac{\partial\overline{\rho'^2}}{\partial x} = -2\,\frac{\overline{u'\rho'}}{\overline{u}}\,\frac{\partial\overline{\rho}}{\partial x}, \tag{14}$$

with an objective to predict the local peak in $\overline{\rho'^2}$ behind the shock, as seen in Fig. 1. Here, only the production due to mean compression is retained and it needs a closure model for the turbulent mass flux correlation $\overline{\rho'u'}$. This is achieved by appealing to the constituent Kovásznay modes in the post-shock thermodynamic field, as described below.

Sethuraman et al. [29] presents Kovásznay mode decomposition of the post-shock density variance obtained from LIA. It is found that the rapid non-monotonic variation behind the shock is caused by the acoustic transient (in the acoustic adjustment region). The far-field asymptotic value, on the other hand, is mostly due to the post-shock entropy mode and is essentially identical to the peak $\overline{\rho'^2}$ (see Fig. 1). We therefore exploit the isobaric nature of the entropy mode to propose the following closure for the $\overline{\rho'u'}$ correlation

$$p' = 0 \quad \Rightarrow \quad \frac{\rho'}{\overline{\rho}} = -\frac{T'}{\overline{T}}, \tag{15}$$

$$\overline{\rho'u'} = -\frac{\overline{\rho}}{\overline{T}}\,\overline{u'T'} = -\frac{\overline{\rho}}{\overline{T}}\,C_{uT}\,\frac{k\,\overline{u}}{c_p}, \tag{16}$$

where C_{uT} is given by Eq. (43) in Appendix B. The modeled form of the $\overline{\rho'^2}$ equation therefore takes the form

$$\frac{\partial\overline{\rho'^2}}{\partial x} = -2\,\frac{\overline{\rho}^2}{c_p\,\overline{T}}\,C_{uT}\,\frac{k}{\overline{u}}\,\frac{\partial\overline{u}}{\partial x}, \tag{17}$$

where the conservation of mass, $\overline{\rho}\,\overline{u}$ = constant is used to replace the mean density gradient with that of the shock-normal

mean velocity. Additionally, the conservation of total enthalpy $c_p\,\overline{T}_0 = c_p\,\overline{T} + \dfrac{\overline{u}^2}{2}$ (neglecting the contribution of TKE) is used to integrate the equation across a shock. An approximate closed-form solution for the normalized downstream $\overline{\rho'^2}$ obtained by assuming $c_p\,\overline{T} = c_p\,\overline{T}_0$ is given by

$$\overline{\rho_2'^2}_{norm.} = \frac{\overline{\rho'^2}}{\overline{\rho}_2^2\,(k_1/\overline{u}_1^2)} \simeq \frac{6\,C_{uT}}{(b_1'-4)}\left[r^{-2} - r^{\frac{2}{3}(1-b_1')}\right]\left[\frac{(\gamma-1)\;M_1^2}{2+(\gamma-1)\;M_1^2}\right], \tag{18}$$

and it is found to match the peak $\overline{\rho'^2}$ in the DNS data well (see Fig. 5). The only exception is Mach 3.5 interaction and the reason for the discrepancy is currently unknown. The model over predicts the LIA far-field data, and does not reproduce the qualitative trend in the limit $M_1 \to 1$. This is similar to that observed for the temperature variance and can be attributed to dropping the dilatation term in the governing equation (13). We note that the high-Mach number limiting value of the normalized $\overline{\rho'^2}$ is bound by unity. This implies that the maximum rms density fluctuations relative to the post-shock mean density cannot exceed the turbulence intensity $u'_{rms}/\overline{u}$ in the upstream flow by a factor of $\sqrt{3/2}$. A more elaborate closed-form solution of Eq. (17) is presented in Appendix C, and it follows the same qualitative trends as the approximate solution given above.

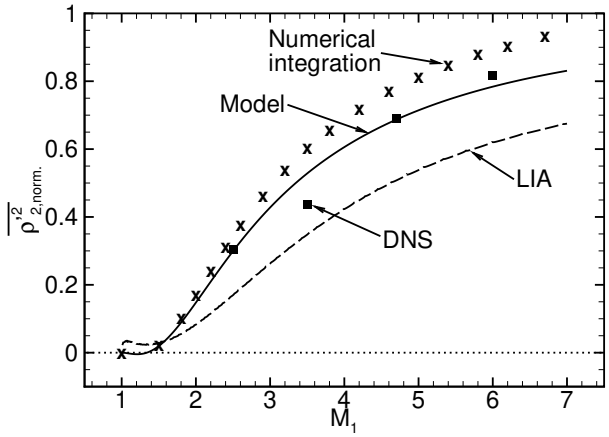

Fig. 5 Mach number variation of normalized density variance from the DNS (post-shock peak value), the LIA far-field and the model predictions (18)**. Normalization is by the factor,** $\overline{\rho}_2^2\,(k_1/\overline{u}_1^2)$**.**

The model equation can be numerically integrated (17) for a prescribed mean velocity profile across a normal shock, as per the procedure described in Appendix D. The results are presented in Fig. 5 (crosses) for the entire range of Mach numbers, and they are higher than the approximate closed-form solution given in Eq. (18) by 10 to 12%. A similar exercise of numerically integrating the model equations for temperature and pressure variances give results that are identical to the respective closed-form solutions, and hence are not presented.

D. Entropy variance

Entropy is a derived quantity, and its dependence on the thermodynamic pressure and density allows us to model its variance using the models developed for the pressure and the density variances. The entropy fluctuations can be written in a linearized form as

$$\frac{s'}{c_p} = \frac{p'}{\gamma\,\overline{p}} - \frac{\rho'}{\overline{\rho}}. \tag{19}$$

and we use it to propose the following model transport equation for $\overline{s'^2}$

$$\frac{\partial}{\partial x}\left(\frac{\overline{s'^2}}{c_p^2}\right) = \frac{1}{\gamma^2}\frac{\partial}{\partial x}\left(\frac{\overline{p'^2}}{\overline{p}^2}\right) + \frac{\partial}{\partial x}\left(\frac{\overline{\rho'^2}}{\overline{\rho}^2}\right) - \frac{2}{\gamma}\frac{\partial}{\partial x}\left(\frac{\overline{p'\,\rho'}}{\overline{p}\,\overline{\rho}}\right). \tag{20}$$

Separately, the jump in entropy fluctuations can be written using Eq. (19)

$$\frac{s_2' - s_1'}{c_p} = \left(\frac{p_2'}{\gamma\,\overline{p}_2} - \frac{p_1'}{\gamma\,\overline{p}_1}\right) - \left(\frac{\rho_2'}{\overline{\rho}_2} - \frac{\rho_1'}{\overline{\rho}_1}\right), \tag{21}$$

which upon multiplying each of its term by $s_m' = (s_1' + s_2')/2$ yields the change in entropy variance across the shock as

$$\frac{\overline{s_2'^2} - \overline{s_1'^2}}{c_p^2} = \underbrace{\frac{1}{\gamma^2}\left(\frac{\overline{p_2'^2}}{\overline{p}_2^2} - \frac{\overline{p_1'^2}}{\overline{p}_1^2}\right)}_{\text{Pressure term}} + \underbrace{\left(\frac{\overline{\rho_2'^2}}{\overline{\rho}_2^2} - \frac{\overline{\rho_1'^2}}{\overline{\rho}_1^2}\right)}_{\text{Density term}} - \underbrace{\frac{2}{\gamma}\left(\frac{\overline{\rho_2'\,p_2'}}{\overline{\rho}_2\,\overline{\rho}_2} - \frac{\overline{\rho_1'\,p_1'}}{\overline{\rho}_1\overline{p}_1}\right)}_{\text{Pressure-density term}}. \tag{22}$$

We use the LIA solution to compute the terms on the right-hand side to obtain the integrated budget of the model equation (20) across a shock wave. The procedure is similar to that described for temperature variance in Sec. III.A. The data is plotted in Fig. 6, where the LIA far-field values of pressure and density fluctuations are used, so as to avoid the near-field LIA data dominated by the acoustic mode.

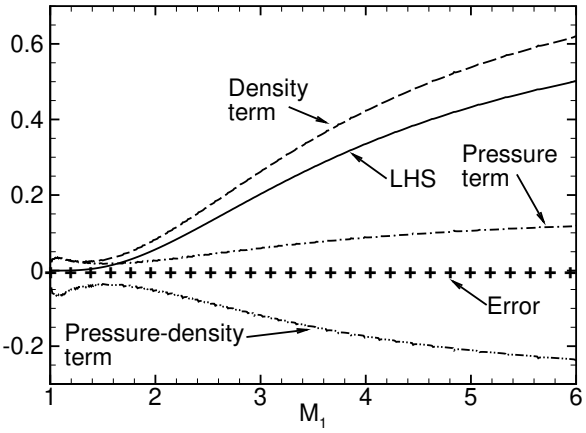

Fig. 6 Budget of Eq. (22) across a normal shock for varying Mach numbers.

We see that the change in entropy variance across the shock is mostly due to the contribution of the density variance term. The pressure variance term is comparatively small and the pressure-density correlation term is negative. The difference between the LHS and the RHS is shown by the error term and is essentially zero for the entire Mach number range. The density variance also reproduces the qualitative trend in the entropy variance closely for $M > 1.5$. This motivates us to retain only the density term in Eq. (20) and write a simple model equation for the entropy variance.

$$\frac{\partial}{\partial x}\left(\frac{\overline{s'^2}}{c_p^2}\right) \simeq \frac{\partial}{\partial x}\left(\frac{\overline{\rho'^2}}{\overline{\rho}^2}\right) \simeq \frac{1}{\overline{\rho}_2^2}\,\frac{\partial \overline{\rho'^2}}{\partial x}. \tag{23}$$

Note that the dependence on the square of the mean density is replaced by its downstream value. This is based on the fact that $\rho_1' \simeq 0$ in a vortical upstream turbulence, such that only the downstream term $\overline{\rho_2'^2}/\overline{\rho}_2^2$ in Eq. (22) contributes to the entropy budget.

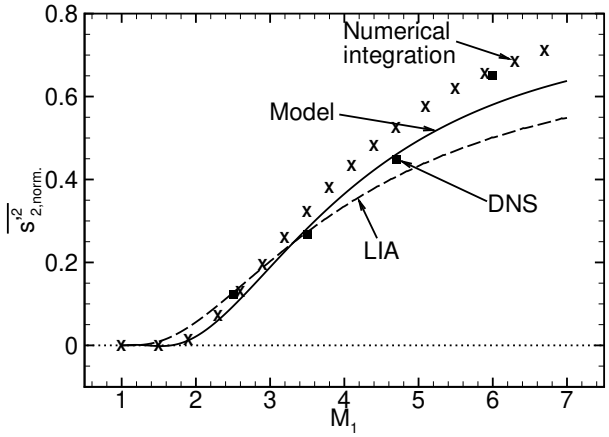

Fig. 7 Variation of normalized entropy variance against Mach number from LIA, DNS (at downstream edge of mean shock) and the model equation ($C_{s1}\times$ Eq. (18)). Normalization is by the factor, $c_p^2\,(k_1/\overline{u}_1^2)$.

A final form of the model equation for entropy variance is thus written as

$$\frac{\partial}{\partial x}\left(\frac{\overline{s'^2}}{c_p^2}\right) \approx C_{s1}\,\frac{\partial \overline{\rho'^2}}{\partial x} = -2\,C_{s1}\,\frac{\overline{\rho}^2}{c_p\,\overline{T}}\,C_{uT}\,\frac{k}{\overline{u}}\,\frac{\partial \overline{u}}{\partial x}, \tag{24}$$

where the production coefficient, $C_{s1} < 1$ accounts for the contribution from the pressure terms in Eq. (22). Additionally, C_{s1} brings in the effect of the density ratio across the shock and is a function of the upstream mean flow Mach number. An approximate closed-form solution for the post-shock entropy variance is equal to C_{s1} times the density variance predicted by Eq. (18), and it is found to match the available DNS data fairly well (see Fig. 7) for the model coefficient

$$C_{s1} = \frac{0.8\,\left(1 - e^{(1-0.6\,M_1)}\right)}{\left(\overline{\rho}_2/\overline{\rho}_1\right)^2}, \tag{25}$$

The model, however, overpredicts compared to the LIA data, especially at high Mach numbers. Numerical integration of Eq. (24) using a specified shock profile (as per Appendix D) gives higher $\overline{s'^2}$ than the approximate closed-form solution. This is similar to the trend observed for the density variance in Fig. 5.

E. Downstream evolution

In this section, we model the downstream evolution of the thermodynamic variances with the physical insights obtained from LIA and DNS. The production mechanism for the thermodynamic variances given by Eqs. (6), (10), (17) and (24) are valid only in the vicinity of the shock wave, since the gradient of mean velocity is zero on either side. In the downstream region, the thermodynamic variances are modeled to mimic the trends observed in the DNS data.

From LIA and DNS profiles of thermodynamic variances in Fig. 1 (Sec. II), it is easy to see that the decay mechanisms are not the same for the four thermodynamic variances. The pressure variance displays a rapid acoustic decay, whereas the entropy variance follows a slower viscous decay. Temperature variance exhibits a mixed type of decay mechanism, which follows the rapid acoustic decay immediately behind the shock up to a distance corresponding to the acoustic lengthscale and a slower decay mechanism similar to the entropy variance beyond the acoustic adjustment region. The production of density variance is modeled by considering its far-field value given by LIA, so as to predict the peak in $\overline{\rho'^2}$ observed in the DNS. Beyond the local peak, the density variance exhibits a decay mechanism similar to the entropy variance.

It is to be noted that the modeled equations for the production of the thermodynamic variances depend on the accurate modeling of TKE, k. Additionally, the dissipation rate of TKE, ϵ is also needed to ensure that the TKE amplified by the shock wave is accurately dissipated. The model equations for k and ϵ from Refs. [8, 31] have proven to predict well for shock-dominated problems. The k (35) and ϵ (38) equations are also integrated simultaneously along with the equations for the thermodynamic variances. For the post-shock flow, they simplify to

$$\overline{u}\,\frac{\partial k}{\partial x} = -\epsilon \quad \text{and} \quad \overline{u}\,\frac{\partial \epsilon}{\partial x} = -C_{\epsilon 2}\,\frac{\epsilon^2}{k}, \tag{26}$$

where the viscous decay of ϵ is modeled in a phenomenological way in terms of the dissipation rate of k. We take a similar approach and model the viscous decay of $\overline{\rho'^2}$ and $\overline{s'^2}$ as

$$\overline{u}\,\frac{\partial \overline{\rho'^2}}{\partial x} = -C_{\rho 1}\,\frac{\epsilon}{k}\,\overline{\rho'^2}, \tag{27}$$

and

$$\overline{u}\,\frac{\partial \overline{s'^2}}{\partial x} = -C_{s2}\,\frac{\epsilon}{k}\,\overline{s'^2}, \tag{28}$$

where $C_{\rho 1}$ and C_{s2} are $O(1)$ coefficients determining the decay rate of the density and entropy variances, respectively.

For the pressure variance, we model the acoustic decay mechanism with the dissipation lengthscale given by $L_\epsilon = k^{3/2}/\epsilon$. The post-shock transport equation is thus written as,

$$\frac{\partial \overline{p'^2}}{\partial x} \sim -\frac{\overline{p'^2}}{L_\epsilon} \simeq -C_{p1}\left(\frac{\overline{p'^2} - \overline{p'^2_\infty}}{L_\epsilon}\right), \tag{29}$$

where $\overline{p'^2_\infty}$ denotes the finite non-zero value of the pressure fluctuations far downstream of the shock. It is prescribed using the asymptotic far-field value obtained from LIA; see Fig. 9a from Ref. [29]. The coefficient C_{p1} controls the rate of decay of pressure variance immediately behind the shock as a fraction of the dissipation lengthscale.

We model the downstream evolution of the temperature variance with a combination of acoustic decay and viscous dissipation,

$$\frac{\partial \overline{T'^2}}{\partial x} = \begin{cases} -C_{T1}\,\frac{\overline{T'^2}}{L_\epsilon} & \text{for} \quad \kappa_0 x \le 1, \\ -C_{T2}\,\frac{1}{\overline{u}}\,\frac{\epsilon}{\overline{u}\,k}\,\overline{T'^2} & \text{for} \quad \kappa_0 x > 1, \end{cases} \tag{30}$$

with a transition at $\kappa_0 x = 1$, which roughly corresponds to the end of the acoustic transient in LIA. The acoustic contribution to $\overline{T'^2}$ is expected to be small beyond this point. The acoustic and viscous decay model coefficients are denoted by C_{T1} and C_{T2}, respectively. They are of $O(1)$, but may vary with Mach number.

IV. Model predictions

The complete equations with the production and the decay terms for each of the thermodynamic variances along with the models for k and ϵ are given below,

$$\overline{u}\,\frac{\partial}{\partial x}\begin{Bmatrix} k \\ \epsilon \\ \overline{T'^2} \\ \overline{\rho'^2} \\ \overline{p'^2} \\ \overline{s'^2} \end{Bmatrix} = -\underbrace{\begin{Bmatrix} \frac{2}{3}\,(1-b_1')\,k\,\frac{\partial \overline{u}}{\partial x} \\ \frac{2}{3}\,C_{\epsilon 1}\,\epsilon\,\frac{\partial \overline{u}}{\partial x} \\ 2\,C_{uT}\,\frac{k\overline{u}^2}{c_{\overline{p}}^2}\,\frac{\partial \overline{u}}{\partial x} \\ 2\,\frac{\overline{\rho}^2}{c_p\,\overline{T}}\,C_{uT}\,k\,\frac{\partial \overline{u}}{\partial x} \\ 2\,\overline{\rho}^2\,C_{uT}\,k\,\overline{u}^2\,\frac{\partial \overline{u}}{\partial x} \\ 2\,C_{s1}\,\frac{c_p}{\overline{T}}\,C_{uT}\,k\,\frac{\partial \overline{u}}{\partial x} \end{Bmatrix}}_{\text{Production}} - \underbrace{\begin{Bmatrix} \epsilon \\ C_{\epsilon 2}\,\frac{\epsilon^2}{k} \\ \Phi \\ C_{\rho 1}\,\frac{\epsilon}{k}\,\overline{\rho'^2} \\ C_{p1}\,\overline{u}\,\left(\frac{\overline{p'^2}-\overline{p'^2_\infty}}{L_\epsilon}\right) \\ C_{s2}\,\frac{\epsilon}{k}\,\overline{s'^2} \end{Bmatrix}}_{\text{Decay}}, \tag{31}$$

where the modeling parameters, $b_1, b_1', C_{\epsilon 1}, C_{\epsilon 2}$ are as provided in Appendix A and C_{uT} is given by Eq. (43) in Appendix B. The other model coefficients in the decay terms are listed below. The decay term in the $\overline{T'^2}$ equation is

given by

$$\Phi = \left(C_{T1}\,\overline{u}\,\frac{\overline{T'^2}}{L_\epsilon} \right) + \left(C_{T2}\,\frac{\epsilon}{k}\,\overline{T'^2} - C_{T1}\,\overline{u}\,\frac{\overline{T'^2}}{L_\epsilon} \right) \frac{1}{2} \left(1 + \tanh\left(x - \frac{1}{2\,\kappa_0} \right) \right), \tag{32}$$

where the hyperbolic tangent function controls the transition from the acoustic decay to the viscous decay. This type of blending function based on lengthscales is similar to the blending functions proposed in the work of Xiao et al. [45], where they used a hyperbolic tangent to shift the numerical method from $k-\zeta$ RANS near the wall to LES with one-equation subgrid scale model away from the wall. A constant value of $\lambda_0/2$ is found to yield reasonably good results for the Mach number range considered in this study.

Table 1 Normalized values of TKE and its dissipation rate for the DNS cases from Larsson et al. [21].

M	M_t	Re_λ	$k_1 \times 10^{-2}$	$\epsilon_1 \times 10^{-4}$	$k_0 \times 10^{-2}$	$\epsilon_0 \times 10^{-4}$
2.5	0.22	40	2.42	9.15	2.66	10.4
3.5	0.22	40	2.42	9.15	2.60	10.0
4.7	0.22	40	2.42	9.15	2.55	9.78
6.0	0.22	40	2.42	9.15	2.52	9.64

The equations (31) are numerically integrated using the mean flow profile provided in Appendix D for the DNS cases of Larsson et al. [21]. Table 1 presents the normalized values of TKE and its dissipation rate at the inlet station (denoted by subscript 0) and just upstream of the shock (denoted by subscript 1) obtained as per the relations provided in Appendix D. Here, k and ϵ are normalized as $k = k^*/\overline{a}_1^{*2}$ and $\epsilon = \epsilon^*/(\overline{a}_1^{*2}\,\kappa_0)$, where $\overline{a}_1$ is the mean speed of sound upstream of the shock with the superscript * denoting dimensional values. The numerical domain extends from $x = -2$ to 8, and is discretized using 10000 points.

The results for the temperature fluctuations are shown in Fig. 8 for the $M = 2.50$, 3.50, 4.70 and 6.00 cases, where $\overline{T'^2}$ is normalized by $\overline{T}_2^2\,(k_1/\overline{u}_1^2)$. The upstream turbulence is essentially vortical in the DNS and it gives negligible temperature variance before the shock ($x < 0$). The grey region around $x = 0$ represents the mean shock thickness and it decreases with increasing Mach number. The production term gives a finite jump in $\overline{T'^2}$ across the shock. It is denoted as the model limiting value without any post-shock decay and it is identical to the model prediction presented in Fig. 3. Introducing the downstream decay gives a lower peak value followed by a rapid decrease up to about $\kappa_0 x = 1$. Subsequently, the model switches to a slower viscous decay beyond $\kappa_0 x = 1$. The coefficients for acoustic decay and viscous dissipation are $C_{T1} = 2 + (M-1)/5$ and $C_{T2} = 0.7 + e^{(1-M)/2}$; they decrease with increasing shock strength.

We next evaluate the model results for density variance in Fig. 9, where both the DNS data and the model predictions are normalized as described in section II. The DNS data for the high Mach number interactions, $M = 4.7$ and 6.0, show a prominent peak in $\overline{\rho'^2}$ at $\kappa_0 x = 1$ behind the shock. The model equation predicts comparable peak values, although its location is shifted to the edge of the mean shock. The post-shock peak in the density variance is less clearly visible for Mach 3.5, because of a higher contribution of the acoustic mode to the density fluctuations in this case. See section (3.3)

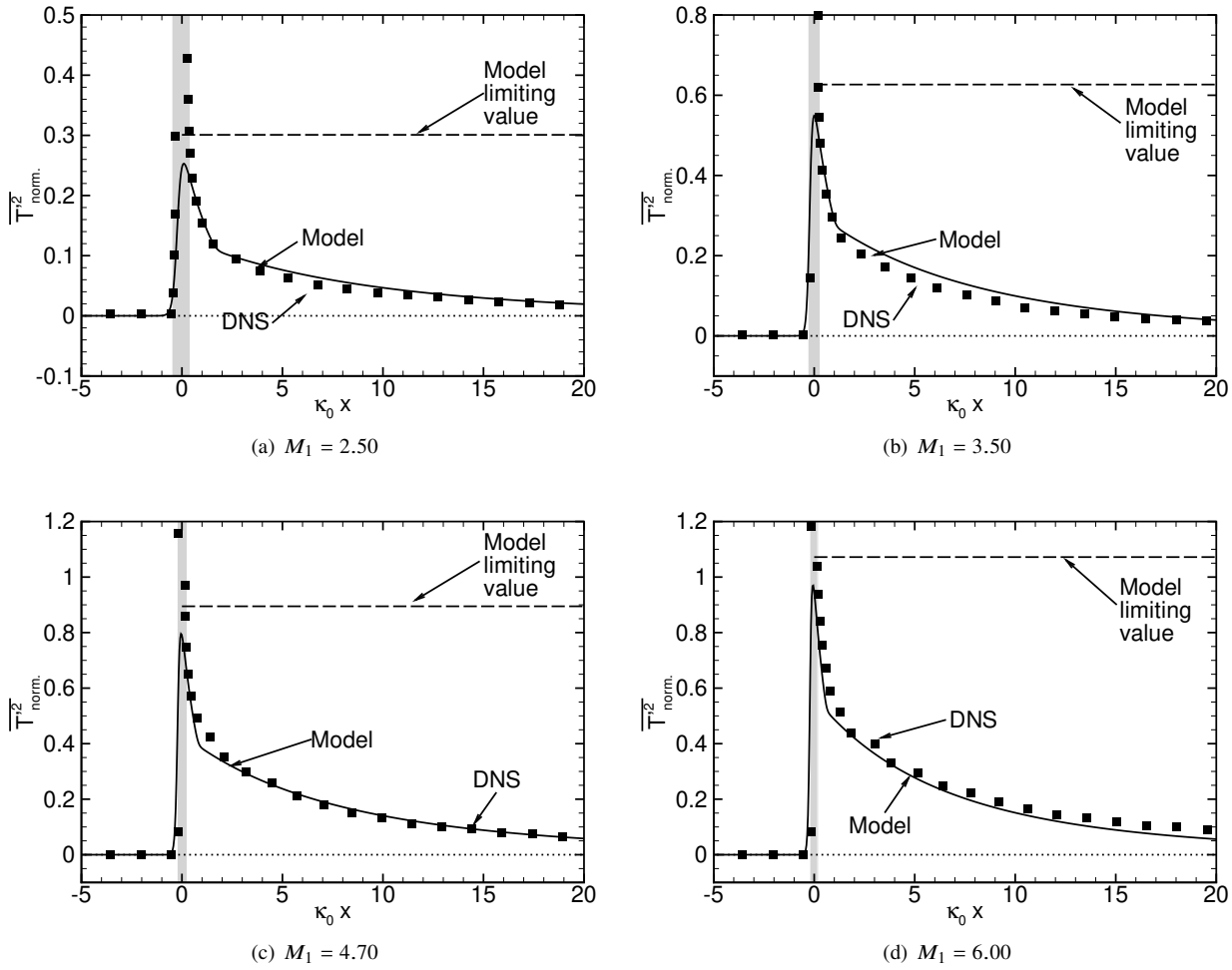

(a) $M_1 = 2.50$ (b) $M_1 = 3.50$

(c) $M_1 = 4.70$ (d) $M_1 = 6.00$

Fig. 8 Comparison of model prediction with DNS data for the variation of $\overline{T'^2}$ with streamwise distance.

in Ref. [29] for additional details. The acoustic effect is even more prominent at Mach 2.5, where the post-shock density variance follows a pattern that resembles the near-field acoustic decay observed for pressure and temperature variances in Fig. 1. For this case, the viscous decay predicted by the model, thus underestimates the rapid drop in $\overline{p'^2}$ in the range $\kappa_0 x < 3$. The model also over predicts the density variance for the Mach 3.5 interaction, but appears to reproduce the downstream decay rate well up to $\kappa_0 x \simeq 8$. By comparison, the DNS data is matched well by the model at Mach 4.7 and 6.0. The model coefficient $C_{\rho 1} = 0.5 + e^{(1-M/2)}$ is used in the model equation.

The pressure variance obtained for the DNS cases of $M = 2.5$, 3.5, 4.7 and 6.0 show identical trend. There is a rapid drop in the near field ($\kappa_0 x < 1$), followed by an asymptotic value further downstream. The model equation reproduces the near-field decay fairly well, for a constant value of the model coefficient $C_{p1} = 2$. The DNS pressure variance further downstream ($\kappa_0 x > 10$) matches the LIA far-field value predicted by the model equation. The model results are lower than the data in the neighbourhood of $\kappa_0 x = 5$, while the model limiting value due to production across the shock overpredicts the DNS data, especially for high Mach numbers. The data presented in Fig. 10, for both the

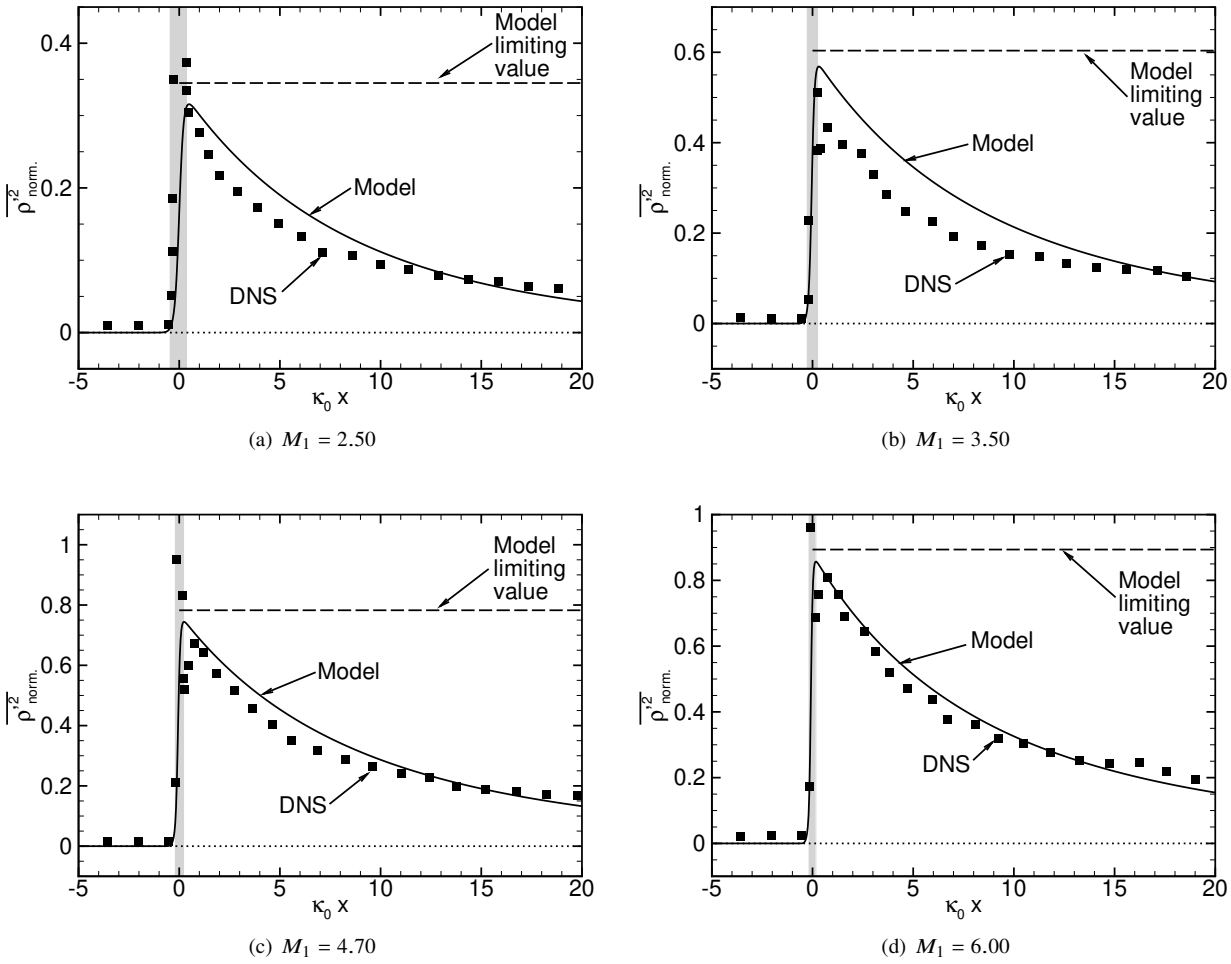

(a) $M_1 = 2.50$ (b) $M_1 = 3.50$

(c) $M_1 = 4.70$ (d) $M_1 = 6.00$

Fig. 9 Model prediction for the streamwise variation of density variance compared with DNS for different Mach numbers.

DNS and the model, follow the normalization presented in section II.

Figure 11 presents an evaluation of the entropy variance model equation against the DNS data. The objective is to compare with the entropy variance outside the grey region of the mean shock wave, and not with the high values in the unsteady shock region. The peak $\overline{s'^2}$ predicted by the model equation is able to match the DNS data well (within 10%) for the high Mach number interactions of 4.7 and 6.0. It is also able to reproduce the DNS entropy variance in the downstream flow, for a constant value of the model coefficient $C_{s2} = 1$. For the $M = 3.5$ case, the model overpredicts the post-shock $\overline{s'^2}$, but matches the post-shock decay rate downstream of the shock. By comparison, the DNS data is underpredicted in the vicinity of the shock wave for Mach 2.5, but overpredicted further downstream. This is due to a mismatch in the decay rate between the DNS and the model equation with $C_{s2} = 1$. A higher viscous dissipation coefficient of $C_{s2} = 1.4$ is able to match the data very well; see Fig. 11(a).

We note that the current model results are obtained for purely vortical turbulence, i.e., negligible entropy variance

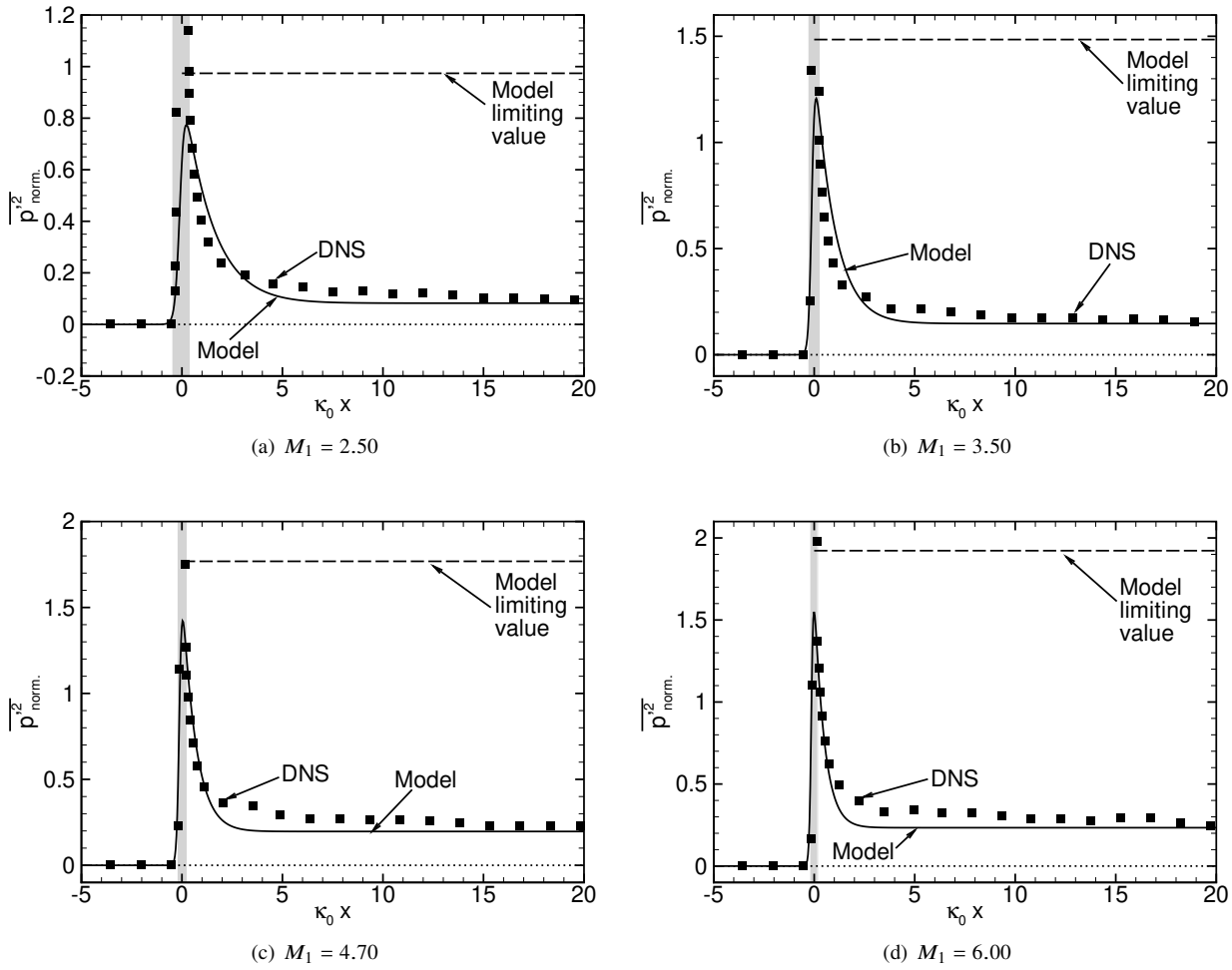

(a) $M_1 = 2.50$

(b) $M_1 = 3.50$

(c) $M_1 = 4.70$

(d) $M_1 = 6.00$

Fig. 10 Spatial variation of the normalized pressure variance obtained from model equation and DNS for different Mach numbers.

upstream of the shock wave. Including the finite value of $\overline{s_1'^2}$ from the DNS would alter the model predictions by a small amount ($4-5\%$). Presence of entropy disturbances in the upstream flow may also bring in additional physics, which is beyond the scope of the current model.

V. Application of the model

The current model tranport equations for the thermodynamic variances are strictly for one-dimensional flow through a normal shock. For a general three-dimensional flow application, the model equations can be cast in a frame-independent form, using the mean dilatation at a shock wave. The left-hand side can be generalized to a convection term, similar to that in a standard $k-\epsilon$ model. The model coefficients are a function of the shock strength in terms of the upstream Mach number, as per the physics of the interaction. For CFD implementation, we can use a shock function of the form proposed in Ref. [43], which can identify the location and strength of the shock waves in the computational domain.

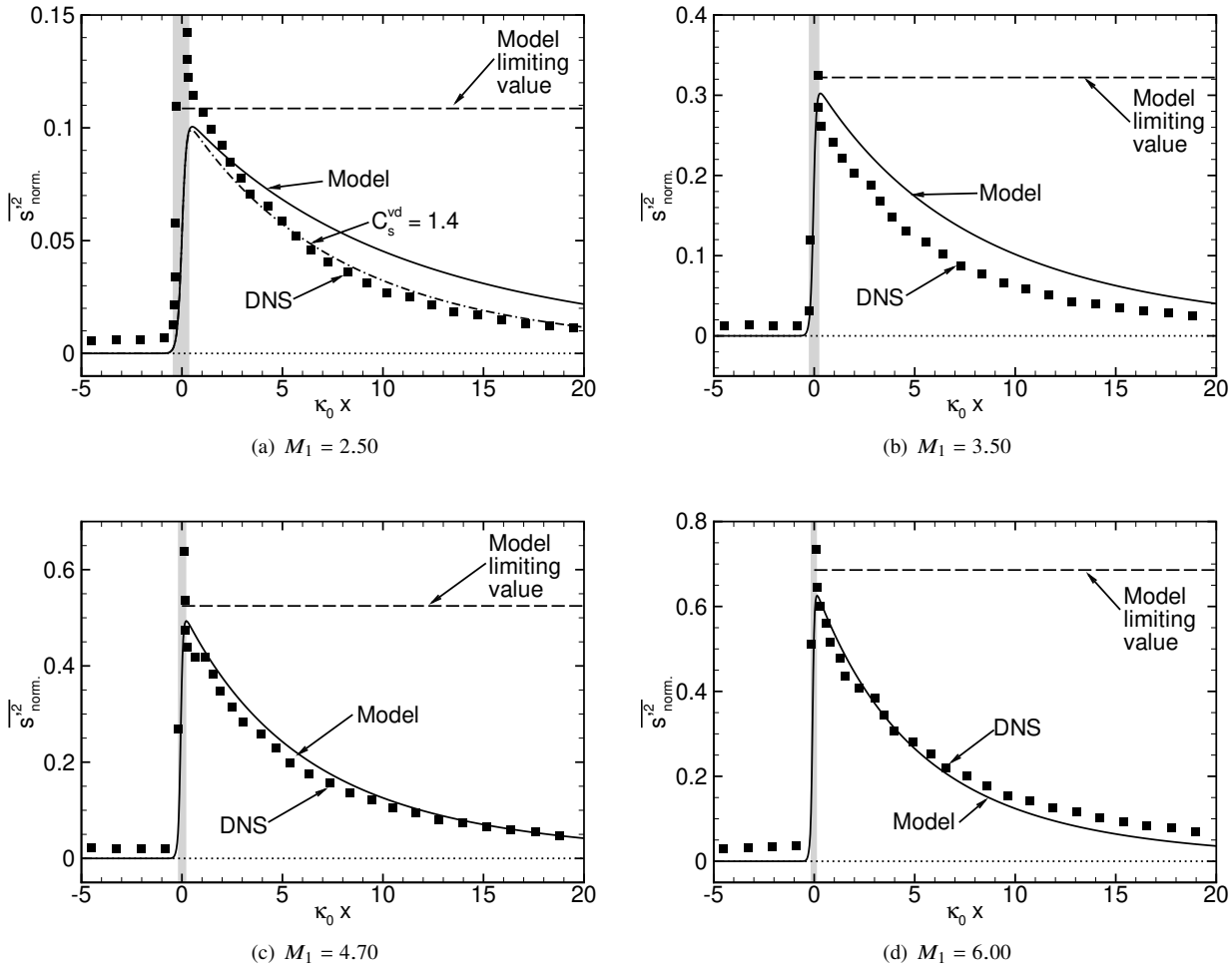

(a) $M_1 = 2.50$

(b) $M_1 = 3.50$

(c) $M_1 = 4.70$

(d) $M_1 = 6.00$

Fig. 11 Variation of the normalized entropy variance in the streamwise direction for different Mach numbers: model vs. DNS.

The mean density ratio r, as well as the ratio of the mean temperature and pressure can thus be calculated.

The transport equation models are primarily intended for use in the RANS framework. The simplicity of the model can be an asset in complex real-life flow configurations, like shock-induced combustion in scramjet engines and plume induced flow separation on space-launch vehicles. The model can also be useful in hybrid methods, like detached eddy simulation, and in RANS-based wall modeling in large eddy simulations. Here, the RANS turbulence model is used in the near wall flow, including the log layer of the boundary layer. Accurate modeling of turbulent fluctuations in the log layer is important for predicting wall properties, like surface heat flux [43].

The model equations predict the post-shock variances in temperature, pressure, density and entropy. These four quantities are expected to characterize the entire thermodynamic field behind the shock. Other relevant quantities, like turbulent mass flux $\overline{\rho' u'}$, temperature flux $\overline{u'T'}$ and the pressure-velocity correlation $\overline{p'u'}$ can be computed using the corresponding correlation coefficients. A case in point is the variable Prandtl number model developed for heat flux

calculation in shock-boundary layer flows. A similar approach can be taken for proposing a variable Schmidt number model for shock-dominated flows.

The modeling methodology followed in the current work uses the linear interaction analysis, which is based on the linear approximation for small fluctuations. This is appropriate for low turbulent Mach number cases. High M_t interactions are found to give higher thermodynamic fluctuations, possibly due to the non-negligible acoustic and entropy fluctuations upstream of the shock wave. The current model for purely vortical incoming turbulence can be extended to higher M_t cases by including the additional acoustic and entropy effects. Here again, LIA results for upstream acoustic and entropy fluctuations have been able to predict the qualitative and quantitative trends with increasing turbulence intensity [46].

VI. Conclusion

In this paper, we propose a turbulence model for predicting the thermodynamic field generated when homogeneous isotropic turbulence interacts with a nominally normal shockwave. The upstream turbulence is assumed to be purely vortical in nature, and the downstream thermodynamic fluctuations are modeled in terms of their constituent acoustic and entropy modes. The model is based on exact transport equations derived at the shock discontinuity, where linear interaction analysis is used to identify the dominant physical processes. Kovásznay mode decomposition is employed to close the source terms at the shock wave. The model predictions for the variances in temperature, pressure, density and entropy are found to match DNS data for a range of Mach numbers. Next, the post-shock evolution of thermodynamics variances is modelled in a phenomenological way in terms of acoustic decay and viscous dissipation, and it reproduces the variation in the downstream flow observed in DNS. The model can be extended to other flows with upstream acoustic and entropy fluctuations. It can also be generalized to oblique shocks and applied to shock-dominated flows in complex configurations.

Appendix

A. Shock-unsteadiness $k-\epsilon$ model

Sinha et al. [31] studied the physics of shock-turbulence interaction in the linear inviscid framework to identify a damping effect of the unsteady shock oscillations on the amplification of TKE across a shock wave. The shock-unsteadiness effect is proportional to the unclosed correlation, $\overline{u'\xi_t}$, which is modeled as

$$\overline{u'\xi_t} = b_1 \, \overline{u'^2}, \tag{33}$$

under the assumption that the unsteady shock motion is caused by the incoming velocity fluctuations. A model transport equation for TKE is developed to capture the shock-unsteadiness physics, and is given by

$$\overline{u}\,\frac{\partial k}{\partial x} = -\overline{u'^2}\,\frac{\partial \overline{u}}{\partial x} + \overline{u'\xi_t}\,\frac{\partial \overline{u}}{\partial x} - \epsilon, \tag{34}$$

where the terms on the right-hand side represent in order, the production of turbulence by mean compression and the second term represents shock-unsteadiness damping. These two terms take large values at a shock wave and determine the amplification of TKE across the shock. The turbulent dissipation rate, ϵ determines the rate of decay of TKE on either side of the shock wave. Using the closure model (Eq. (33)) in the above equation

$$\overline{u}\,\frac{\partial k}{\partial x} = -\frac{2}{3}\,\left[1 - b_1'\right]\,k\,\frac{\partial \overline{u}}{\partial x} - \epsilon, \tag{35}$$

where we use isotropic form of the Reynolds stress, $\overline{u'^2} = \frac{2}{3}\,k$ valid for the upstream field. Also the closure coefficient b_1 in Eq. (33) is modified to b_1' to account for low Mach number effects; $b_1' = b_{1,\infty}\,(1 - e^{1-M_1})$ and $b_{1,\infty} = 0.4$ is the high Mach number limiting value of the coefficient b_1 obtained from LIA. Neglecting the dissipation effect across an infinitely thin shock wave gives the TKE amplification as,

$$\frac{k_2}{k_1} = \left(\frac{\overline{u}_2}{\overline{u}_1}\right)^{-\frac{2}{3}\,(1-b_1')}. \tag{36}$$

It matches DNS data for canonical STI for a range of Mach numbers. See the original reference [31] for additional details.

In another work, Sinha [8] presents a detailed study of the vorticity amplification by shock compression and baroclinic effects. The resulting amplification of enstrophy (the variance of vorticity) and the changes in the kinematic viscosity of the fluid across the shock are used to write the following transport equation for the solenoidal dissipation rate,

$$\frac{\partial \epsilon_s}{\partial x} = \widetilde{u}\,\frac{\partial}{\partial x}\left(\overline{\nu}\,\overline{\omega_i'\omega_i'}\right) = \widetilde{u}\,\overline{\omega_i'\omega_i'}\,\frac{\partial \overline{\nu}}{\partial x} + \overline{\nu}\,\frac{\partial\left(\overline{\omega_i'\omega_i'}\right)}{\partial x}, \tag{37}$$

A model developed for enstrophy amplification is developed using LIA and it is cast in a form similar to the $\epsilon-$ equation in $k-\epsilon$ turbulence model,

$$\overline{\rho}\,\overline{u}\,\frac{\partial \epsilon_s}{\partial x} = -\frac{2}{3}\,C_{\epsilon 1}\,\overline{\rho}\,\epsilon_s\,\frac{\partial \widetilde{u}}{\partial x} - C_{\epsilon 2}\,\overline{\rho}\frac{\epsilon_s^2}{k}, \tag{38}$$

where $C_{\epsilon 1} = 1 + 0.21\,M_1$ and $C_{\epsilon 2} = 1.2$. Once again, the model prediction for ϵ_s is found to match DNS data in canonical shock-turbulence interaction.

B. Model for temperature flux

Quadros & Sinha [42] develop a transport equation model for the turbulent energy flux generated by a shock wave. We follow a similar procedure to obtain a model for the temperature flux, $\overline{u'T'}$ in canonical shock-turbulence interaction. By taking a moment of Eq. (2) in Sec. III with u', we get,

$$c_p \frac{\partial}{\partial x}\left(\overline{u'T'}\right) = -\overline{u}\frac{\partial}{\partial x}\left(\frac{\overline{u'^2}}{2}\right) - \overline{u'^2}\frac{\partial \overline{u}}{\partial x} + \overline{u'\xi_t}\frac{\partial \overline{u}}{\partial x} + c_p\,\overline{T'\frac{\partial u'}{\partial x}}, \tag{39}$$

where the first term on the right-hand side represents the transfer of turbulent kinetic energy to internal energy fluctuations. The second and the third terms appear as the production and shock-unsteadiness terms in TKE equation (Eq. (34)). The last term is the temperature-dilatation correlation. Assuming $\overline{u'^2} = 2k/3$ and $\overline{u'\xi_t} = b_1\overline{u'^2}$, as in Appendix A, we can rewrite Eq. (39) as,

$$c_p \frac{\partial}{\partial x}\left(\overline{u'T'}\right) = -\frac{2}{9}\left(2 + b_1' - 3\,b_1\right)\,k\,\frac{\partial \overline{u}}{\partial x} + c_p\,\overline{T'\frac{\partial u'}{\partial x}}, \tag{40}$$

The effect of the mean flow gradient is expected to be large. Neglecting the last term and integrating Eq. (40) along with TKE equation (Eq. (35)), without the dissipation term in the vicinity of the shock wave, we get,

$$c_p\,\overline{u_2'T_2'} \approx \left[\frac{2}{9}\left(2 + b_1' - 3\,b_1\right)\right]\left(\frac{3}{2b_1' + 1}\right)\left[1 - r^{-\frac{1}{3}\left(2b_1'+1\right)}\right]\,k_1\,\overline{u}_1, \tag{41}$$

where $T_1' = 0$ for purely vortical upstream turbulence and $r = \overline{u}_1/\overline{u}_2$. The temperature flux generated by the shock is thus proportional to the upstream turbulent kinetic energy and the mean flow velocity of the incoming flow. This is physically consistent with linear interaction analysis, which predicts that all post-shock turbulent correlations scale with the energy of the turbulent velocity fluctuations. Taking this as a guiding principle, we write a model for the variation of the temperature flux across the shock in terms of the local turbulent kinetic energy and the local mean velocity.

$$\overline{u'T'} = C_{uT}\,\frac{k\,\overline{u}}{c_p}, \tag{42}$$

It can thus be used in the model transport equation for the thermodynamic variances and integrated across the shock. Here,

$$C_{uT} = \frac{2}{3}\left(\frac{2 + b_1' - 3\,b_1}{2b_1' + 1}\right)\left[1 - r^{-\frac{1}{3}\left(2b_1'+1\right)}\right], \tag{43}$$

is a function of the shock Mach number, either in terms of the closure coefficient, b_1' and b_1, or via the density ratio r across the shock. A comparison of the model prediction with DNS and LIA results is shown in Fig. 12, where the DNS data behind the shock is extrapolated back to the shock center location. Normalization is by the factor, $\overline{u}_1\,\overline{T}_2\,(k_1/\overline{u}_1^2)$.

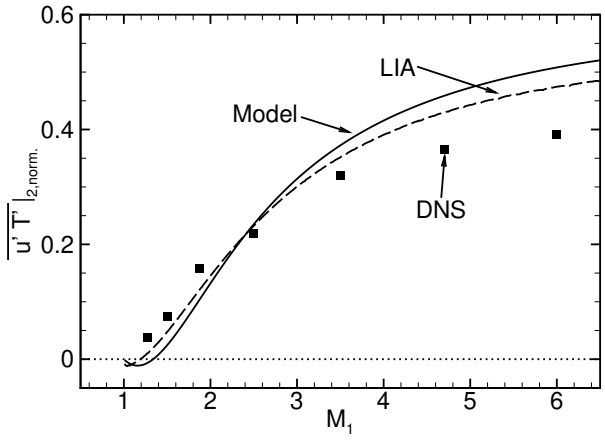

Fig. 12 Variation of normalized temperature flux correlation against Mach number.

C. Full expression for density variance

Integration of Eq. (17) with the assumption $c_p\,\overline{T} = c_p\,\overline{T}_0$ and suitable normalization results in Eq. (18). On the other hand, substituting $c_p\,\overline{T}$ as $c_p\,\overline{T}_0 - (\overline{u}^2/2)$, following the conservation of total enthalpy in Eq. (17) yields,

$$\frac{\partial\overline{\rho'^2}}{\partial x} = -2\,\frac{\overline{\rho}^2}{c_p\,\overline{T}_0}\left(1 - \frac{\overline{u}^2}{c_p\,\overline{T}_0}\right) C_{uT}\,\frac{k}{\overline{u}}\,\frac{\partial\overline{u}}{\partial x}, \tag{44}$$

where we have limited the binomial expansion of $(c_p\overline{T})^{-1}$ in Eq. (17) up to first order terms only. Integrating and normalizing as performed for Eq. (18) gives,

$$\begin{aligned}\left(\overline{\rho_2'^2}\right)_{norm.} = \frac{\overline{\rho'^2}}{\overline{\rho}_2^2\,(k_1/\overline{u}_1^2)} \simeq \frac{6\,C_{uT}}{r^2}\left[\frac{(\gamma-1)\;M_1^2}{2+(\gamma-1)\;M_1^2}\right]\times \\ \left\{\left(\frac{1}{b_1'-4}\right)\left[1 - r^{-\frac{2}{3}(b_1'-4)}\right] + \left[\frac{(\gamma-1)\;M_1^2}{2+(\gamma-1)\;M_1^2}\right]\left(\frac{1}{b_1'-1}\right)\left[1 - r^{-\frac{2}{3}(b_1'-1)}\right]\right\},\end{aligned} \tag{45}$$

Figure 13 compares the predictions of Eq. (18) and Eq. (45), where it is found that the approximation of $c_p\,\overline{T} = c_p\,\overline{T}_0$ is reasonably valid. The largest error is approximately 8% at $M_1 = 7$. Further expansion of the series in $(c_p\overline{T})^{-1}$ is found to show no significant increase in the model predictions of density variance.

D. Numerical integration across the shock profile

The canonical nature of the model problem reduces the dimensionality of the statistics, i.e., the averages and variances vary only in the streamwise direction. This enables us to solve the modeled transport equations for the TKE, its dissipation rate, and the thermodynamic variances given in Eq. (31) in a one-dimensional framework. The partial differential operator (∂) and the ordinary differential operator (d) mean the same in this framework, and are used interchangeably. The equations are integrated in space using the classical 4^{th} order accurate Runge-Kutta method. The

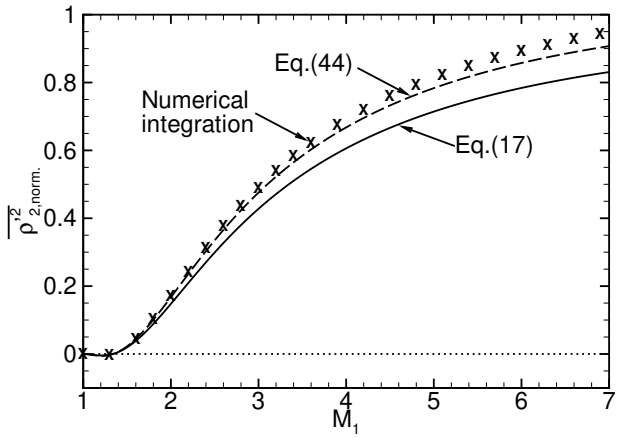

Fig. 13 Variation of normalized density variance similar to Fig. 5 comparing the predictions from Eq. (18)**, Eq.** (45) **and the numerical integration of Eq.** (17)**.**

mean profile with the shock located at $\kappa_0 x = 0$ is specified as follows,

$$\overline{u}(x) = \overline{u}_1 + (\overline{u}_2 - \overline{u}_1)\ \frac{1}{2}\ (1 + \tanh(x)), \tag{46}$$

$$\overline{\rho}(x) = \overline{\rho}_1\ \frac{\overline{u}_1}{\overline{u}(x)}, \tag{47}$$

$$\overline{T}(x) = \overline{T}_1 + \frac{1}{2c_p}\ \left(\overline{u}_1^2 - \overline{u}(x)^2\right), \tag{48}$$

$$\frac{\mathrm{d}\overline{u}(x)}{\mathrm{d}x} = \frac{\overline{u}_2 - \overline{u}_1}{\Delta x}\ \frac{1}{2}\ \left(1 - \tanh^2(x)\right), \tag{49}$$

$$\frac{\mathrm{d}\overline{T}(x)}{\mathrm{d}x} = -\frac{1}{c_p}\ \overline{u}(x)\ \frac{\mathrm{d}\overline{u}(x)}{\mathrm{d}x}, \tag{50}$$

where Δx is the uniform grid spacing in the one-dimensional grid. A total of 10000 points is used in the domain of integration.

The equations given in Eq. (31) are integrated in their non-dimensional form as shown below,

$$u = \frac{u^*}{a_1^*}, \quad T = \frac{T^*}{T_1^*(\gamma - 1)}, \quad \rho = \frac{\rho^*}{\rho_1^*}, \quad p = \frac{p^*}{p_1^*\gamma}, \quad s = \frac{s^*}{c_p^*} \quad R = \frac{R^*}{c_p^*} = \frac{\gamma - 1}{\gamma}, \quad c_p = \frac{c_p^*}{c_p^*} = 1, \tag{51}$$

with the superscript * denoting dimensional quantities. The values of k and ϵ at the inlet of the one-dimensional domain are obtained by linearly extrapolating the DNS values from the location just upstream of the shock to the inlet station using the relation of homogeneous isotropic turbulence decaying without any mean strain, as mentioned in Ref. [47]. The expressions for computing the inlet values of k and ϵ are

$$\kappa_0 = k_1\ \left[1 + \frac{x_{sh.}\ \epsilon_0}{\overline{u}_1\ n}\right]^n, \quad \epsilon_0 = \epsilon_1\ \left[1 + \frac{x_{sh.}\ \epsilon_0}{\overline{u}_1\ n}\right]^{n+1}, \tag{52}$$

where, $n = 1/(C_{\epsilon 2} - 1)$ is the decay exponent with $C_{\epsilon 2} = 1.2$ and $\kappa_0 x_{sh.} = 6.83$ is the normalized distance of the shock from the inlet station. The domain spans from $\kappa_0 x = -7.6$ at the inlet to the exit at $\kappa_0 x = 29.6$.

The values of k and ϵ at the location just upstream of the shock need to be known *a priori*, and are computed as,

$$k_1 = \frac{M_t^2}{2}, \quad \epsilon_1 = \frac{5\, M_t^3}{\sqrt{3}\,(\kappa_0 \lambda^*)\, Re_\lambda}, \tag{53}$$

where λ^* is the dimensional Taylor lengthscale. The values of M_t and Re_λ are set as per the available DNS data. The values of $\overline{\rho'^2}$, $\overline{p'^2}$, $\overline{T'^2}$ and $\overline{s'^2}$ at the inlet are set to zero as per the assumption of purely vortical turbulence upstream of the shock. Extrapolation condition is considered for the outflow boundary in this study.

Acknowledgments

We thank Dr. Johan Larsson, University of Maryland, College Park, USA for the DNS data.

References

[1] Urzay, J., "Supersonic Combustion in Air-Breathing Propulsion Systems for Hypersonic Flight," *Annual Review of Fluid Mechanics*, Vol. 50, No. 1, 2018, pp. 593–627. doi:10.1146/annurev-fluid-122316-045217.

[2] Bhagatwala, A. V., "Shock-turbulence interaction and Richtmyer-Meshkov instability in spherical geometry," Ph.D. thesis, Stanford University, 2011.

[3] Soulard, O., Griffond, J., and Souffland, D., "Pseudocompressible approximation and statistical turbulence modeling: Application to shock tube flows," *Physical Review E*, Vol. 85, No. 2, 2012, p. 026307. doi:10.1103/PhysRevE.85.026307.

[4] Abdikamalov, E., Zhaksylykov, A., Radice, D., and Berdibek, S., "Shock-turbulence interaction in core-collapse supernovae," *Monthly Notices of the Royal Astronomical Society*, Vol. 461, No. 4, 2016, pp. 3864–3876. doi:10.1093/mnras/stw1604.

[5] Huete, C., Abdikamalov, E., and Radice, D., "The impact of vorticity waves on the shock dynamics in core-collapse supernovae," *Monthly Notices of the Royal Astronomical Society*, Vol. 475, No. 3, 2018, pp. 3305–3323. doi:10.1093/mnras/stx3360.

[6] Tian, Y., Jaberi, F. A., Li, Z., and Livescu, D., "Numerical study of variable density turbulence interaction with a normal shock wave," *Journal of Fluid Mechanics*, Vol. 829, 2017, pp. 551–588. doi:10.1017/jfm.2017.542.

[7] Karl, S., Hickey, J.-P., and Lacombe, F., "Reynolds Stress Models for Shock-Turbulence Interaction," *31st International Symposium on Shock Waves 1*, edited by A. Sasoh, T. Aoki, and M. Katayama, Fundamentals, Springer International Publishing, 2019, pp. 511 – 517. doi:10.1007/978-3-319-91020-8.

[8] Sinha, K., "Evolution of enstrophy in shock/homogeneous turbulence interaction," *Journal of Fluid Mechanics*, Vol. 707, 2012, pp. 74 – 110. doi:10.1017/jfm.2012.265.

[9] Quadros, R., Sinha, K., and Larsson, J., "Turbulent energy flux generated by shock/homogeneous-turbulence interaction," *Journal of Fluid Mechanics*, Vol. 796, 2016, pp. 113 – 157. doi:10.1017/jfm.2016.236.

[10] Lee, S., Lele, S. K., and Moin, P., "Direct numerical simulation of isotropic turbulence interacting with a weak shock wave," *Journal of Fluid Mechanics*, Vol. 251, 1993, pp. 533 – 562. doi:10.1017/S0022112093003519.

[11] Mahesh, K., Lele, S. K., and Moin, P., "The influence of entropy fluctuations on the interaction of turbulence with a shock wave," *Journal of Fluid Mechanics*, Vol. 334, 1997, pp. 353 – 379. doi:10.1017/S0022112097004576.

[12] Larsson, J., Bermejo-Moreno, I., and Lele, S. K., "Reynolds-and Mach-number effects in canonical shock-turbulence interaction," *Journal of Fluid Mechanics*, Vol. 717, 2013, pp. 293 – 321. doi:10.1017/jfm.2012.573.

[13] Wouchuk, J. G., Huete Ruiz de Lira, C., and Velikovich, A. L., "Analytical linear theory for the interaction of a planar shock wave with an isotropic turbulent vorticity field," *Physical Review E*, Vol. 79, No. 6, 2009, p. 066315. doi:10.1103/PhysRevE.79.066315.

[14] Huete Ruiz de Lira, C., Velikovich, A. L., and Wouchuk, J. G., "Analytical linear theory for the interaction of a planar shock wave with a two- or three-dimensional random isotropic density field," *Physical Review E*, Vol. 83, No. 5, 2011, p. 056320. doi:10.1103/PhysRevE.83.056320.

[15] Huete, C., Wouchuk, J. G., and Velikovich, A. L., "Analytical linear theory for the interaction of a planar shock wave with a two- or three-dimensional random isotropic acoustic wave field," *Physical Review E*, Vol. 85, No. 2, 2012, p. 026312. doi:10.1103/PhysRevE.85.026312.

[16] Farag, G., Boivin, P., and Sagaut, P., "Interaction of two-dimensional spots with a heat releasing/absorbing shock wave: linear interaction approximation results," *Journal of Fluid Mechanics*, Vol. 871, 2019, pp. 865 – 895. doi:10.1017/jfm.2019.324.

[17] Barre, S., Alem, D., and Bonnet, J. P., "Experimental study of a normal shock / homogeneous turbulence interaction," *AIAA Journal*, Vol. 34, No. 5, 1996, pp. 968 – 974. doi:10.2514/3.13175.

[18] Agui, J. H., Briassulis, G., and Andreopoulos, Y., "Studies of interactions of a propagating shock wave with decaying grid turbulence: velocity and vorticity fields," *Journal of Fluid Mechanics*, Vol. 524, 2005, pp. 143–195. doi:10.1017/S0022112004002514.

[19] Kitamura, T., Nagata, K., Sakai, Y., Sasoh, A., and Ito, Y., "Changes in divergence-free grid turbulence interacting with a weak spherical shock wave," *Physics of Fluids*, Vol. 29, No. 6, 2017, p. 065114. doi:10.1063/1.4984835.

[20] Mahesh, K., Moin, P., and Lele, S. K., "The interaction of a shock wave with a turbulent shear flow," Tech. Rep. TF-69, Thermosciences Division, Department of Mechanical Engineering, Stanford University, Stanford, California 94305, 1996.

[21] Larsson, J., and Lele, S. K., "Direct numerical simulation of canonical shock/turbulence interaction," *Physics of Fluids*, Vol. 21, No. 12, 2009, p. 126101. doi:10.1063/1.3275856.

[22] Lele, S. K., "Compressibility Effects on Turbulence," *Annual Review of Fluid Mechanics*, Vol. 26, No. 1, 1994, pp. 211 – 254. doi:10.1146/annurev.fl.26.010194.001235.

[23] Ribner, H. S., "Acoustic energy flux from shock-turbulence interaction," *Journal of Fluid Mechanics*, Vol. 35, No. 2, 1969, p. 299–310. doi:10.1017/S0022112069001121.

[24] Ribner, H. S., "Spectra of noise and amplified turbulence emanating from shock-turbulence interaction," *AIAA Journal*, Vol. 25, No. 3, 1987, pp. 436 – 442. doi:10.2514/3.9642.

[25] Schülein, E., "Skin-Friction and Heat Flux Measurements in Shock / Boundary-Layer Interaction Flows," *AIAA Journal*, Vol. 44, No. 8, 2006, pp. 1732 – 1741. doi:10.2514/1.15110.

[26] Martínez Ferrer, P. J., Buttay, R., Lehnasch, G., and Mura, A., "A detailed verification procedure for compressible reactive multicomponent Navier-Stokes solvers," *Computers and Fluids*, Vol. 89, 2014, pp. 88 – 110. doi:10.1016/j.compfluid.2013.10.014.

[27] Mathieu, O., Pemelton, J. M., Bourque, G., and Petersen, E. L., "Shock-induced ignition of methane sensitized by NO_2 and N_2O," *Combustion and Flame*, Vol. 162, No. 8, 2015, pp. 3053 – 3070. doi:10.1016/j.combustflame.2015.03.024.

[28] Huete, C., Sánchez, A. L., Williams, F. A., and Urzay, J., "Diffusion-flame ignition by shock-wave impingement on a supersonic mixing layer," *Journal of Fluid Mechanics*, Vol. 784, 2015, pp. 74 – 108. doi:10.1017/jfm.2015.585.

[29] Sethuraman, Y. P. M., Sinha, K., and Larsson, J., "Thermodynamic fluctuations in canonical shock–turbulence interaction: effect of shock strength," *Theoretical and Computational Fluid Dynamics*, Vol. 32, No. 5, 2018, pp. 629 – 654. doi:10.1007/s00162-018-0468-y.

[30] Kovásznay, L. S. G., "Turbulence in Supersonic Flow," *Journal of the Aeronautical Sciences*, Vol. 20, No. 10, 1953, pp. 657 – 674, 682. Reprinted in *AIAA Journal*, **41(7)**, 219-237, 2003.

[31] Sinha, K., Mahesh, K., and Candler, G. V., "Modeling shock unsteadiness in shock/turbulence interaction," *Physics of Fluids*, Vol. 15, No. 8, 2003, pp. 2290 – 2297. doi:10.1063/1.1588306.

[32] Emami, B., Bussmann, M., and Tran, H., "Application of Realizability and Shock Unsteadiness $k - \epsilon$ to Simulations of Under-Expanded Axisymmetric Supersonic Free Jets," *Journal of Fluids Engineering*, Vol. 132, No. 4, 2010. doi:10.1115/1.4001341, 041104.

[33] Morgan, B. E., and Wickett, M. E., "Three-equation model for the self-similar growth of Rayleigh-Taylor and Richtmyer-Meskov instabilities," *Physical Review E*, Vol. 91, 2015, p. 043002. doi:10.1103/PhysRevE.91.043002.

[34] Schwarzkopf, J. D., Livescu, D., Baltzer, J. R., Gore, R. A., and Ristorcelli, J. R., "A Two-length Scale Turbulence Model for Single-phase Multi-fluid Mixing," *Flow Turbulence and Combustion*, Vol. 96, No. 1, 2016, pp. 1 – 43. doi:10.1007/s10494-015-9643-z.

[35] Zhang, Z., Gao, Z., Jiang, C., and Lee, C.-H., "A RANS model correction on unphysical over-prediction of turbulent quantities across shock wave," *International Journal of Heat and Mass Transfer*, Vol. 106, 2017, pp. 1107 – 1119. doi:10.1016/j.ijheatmasstransfer.2016.10.087.

[36] Zhou, Y., "Rayleigh - Taylor and Richtmyer - Meshkov instability induced flow, turbulence, and mixing. II," *Physics Reports*, Vol. 723 - 725, 2017, pp. 1 – 160. doi:10.1016/j.physrep.2017.07.008.

[37] Roy, S., and Sinha, K., "Turbulent Heat Flux Model for Hypersonic Shock–Boundary Layer Interaction," *AIAA Journal*, Vol. 57, No. 8, 2019, pp. 3624 – 3629. doi:10.2514/1.J058334.

[38] Vyas, M. A., Yoder, D. A., and Gaitonde, D. V., "Reynolds-Stress Budgets in an Impinging Shock-Wave/Boundary-Layer Interaction," *AIAA Journal*, 2019, pp. 1–17. doi:10.2514/1.J058487, Published online 31 Jul. 2019. Article in Advance.

[39] Taulbee, D., and VanOsdol, J., "Modeling Turbulent Compressible Flows: The Mass Fluctuating Velocity and Squared Density," *29th Aerosp. Sci. Meet.*, Reno, NV, USA, 1991, pp. 1–9. doi:10.2514/6.1991-524.

[40] Xiao, X., Hassan, H. A., Edwards, J. R., and Gaffney Jr., R. L., "Role of Turbulent Prandtl Numbers on Heat Flux at Hypersonic Mach Numbers," *AIAA Journal*, Vol. 45, No. 4, 2007, pp. 806 – 813. doi:10.2514/1.21447.

[41] Schwarzkopf, J. D., Livescu, D., Gore, R. A., Rauenzahn, R. M., and Ristorcelli, J. R., "Application of a second-moment closure model to mixing processes involving multicomponent miscible fluids," *Journal of Turbulence*, Vol. 12, No. 49, 2011, pp. 1–35. doi:10.1080/14685248.2011.633084.

[42] Quadros, R., and Sinha, K., "Modelling of turbulent energy flux in canonical shock-turbulence interaction," *International Journal of Heat and Fluid Flow*, Vol. 61, Part B, 2016, pp. 626 – 635. doi:10.1016/j.ijheatfluidflow.2016.07.006.

[43] Roy, S., Pathak, U., and Sinha, K., "Variable Turbulent Prandtl Number Model for Shock / Boundary - Layer Interaction," *AIAA Journal*, Vol. 56, No. 1, 2018, pp. 342–355. doi:10.2514/1.J056183.

[44] Sinha, K., and Yogesh Prasaad, M. S., "Analysis and modeling of thermodynamic fluctuations generated by shock-turbulence interaction," *AIAA Scitech 2019 Forum, AIAA 2019-2155*, San Diego, CA, USA, 2019, pp. 1–19. doi:10.2514/6.2019-2155.

[45] Xiao, X., Edwards, J. R., and Hassan, H. A., "Blending Functions in Hybrid Large-Eddy / Reynolds-Averaged Navier-Stokes Simulations," *AIAA Journal*, Vol. 42, No. 12, 2004, pp. 2508 – 2515. doi:10.2514/1.2094.

[46] Sethuraman, Y. P. M., and Sinha, K., "Effect of turbulent Mach number on the thermodynamic fluctuations in canonical shock-turbulence interaction," *Computers and Fluids*, 2019. Under Review.

[47] Raje, P., and Sinha, K., "A physically consistent and numerically robust $k - \epsilon$ model for computing turbulent flows with shock waves," *Computers and Fluids*, Vol. 136, 2016, pp. 35 – 47. doi:10.1016/j.compfluid.2016.05.026.